LARGE-SCALE BIOLOGY

Multi-omics analysis reveals the molecular mechanisms underlying virulence in *Rhizoctonia* and jasmonic acid–mediated resistance in Tartary buckwheat (*Fagopyrum tataricum*)

Yuqi He,[a,b,1] Kaixuan Zhang,[a,1] Shijuan Li,[a,c,1] Xiang Lu,[a,d,1] Hui Zhao,[a,1] Chaonan Guan,[a,b,1] Xu Huang[a,1], Yaliang Shi,[a] Zhen Kang,[a] Yu Fan,[a] Wei Li,[a] Cheng Chen,[a] Guangsheng Li,[a] Ou Long,[a] Yuanyuan Chen,[a] Mang Hu,[a] Jianping Cheng,[d] Bingliang Xu,[c] Mark A. Chapman,[e] Milen I Georgiev,[f,g] Alisdair R. Fernie,[g,h] Meiliang Zhou[a,b,2]

[a] Institute of Crop Sciences, Chinese Academy of Agricultural Sciences, National Crop Gene Bank Building, Zhongguancun South Street No. 12, Haidian District, Beijing 100081, China.
[b] National Nanfan Research Institute, Chinese Academy of Agricultural Sciences, Sanya 572024, China.
[c] College of Plant Protection, Gansu Agricultural University, Lanzhou 730070, China.
[d] College of Agriculture, Guizhou University, Guiyang 550025, China.
[e] Biological Sciences, University of Southampton, Life Sciences Building 85, Highfield Campus, Southampton, SO17 1BJ, UK.
[f] Laboratory of Metabolomics, Institute of Microbiology, Bulgarian Academy of Sciences, 4000 Plovdiv, Bulgaria.
[g] Center of Plant Systems Biology and Biotechnology, 4000 Plovdiv, Bulgaria.
[h] Department of Molecular Physiology, Max-Planck-Institute of Molecular Plant Physiology, Am Mühlenberg 1, 14476 Potsdam-Golm, Germany.

[1] These authors contributed equally to this work.
[2] Corresponding author: zhoumeiliang@caas.cn

Short title: Genetic resistance against *R. solani* in buckwheat

One-sentence summary: Multi-omics association analysis dissects the genetic basis of the virulence mechanism in *Rhizoctonia solani* and the jasmonic acid-mediated resistance against *Rhizoctonia solani* in Tartary buckwheat.

The author responsible for distribution of materials integral to the findings presented in this article in accordance with the policy described in the instructions for authors (https://academic.oup.com/plcell/) is: Meiliang Zhou (zhoumeiliang@caas.cn).

ABSTRACT

Rhizoctonia solani is a devastating soil-borne pathogen that seriously threatens the cultivation of economically important crops. Multiple strains with a very broad host range have been identified, but only one (AG1-IA, which causes rice sheath blight disease) has been examined in detail. Here, we analyzed AG4-HGI 3 originally isolated from Tartary buckwheat (*Fagopyrum tataricum*), but with a host range comparable to AG1-IA. Genome comparison reveals abundant pathogenicity genes in this strain. We used multi-omics approaches to improve the efficiency of screening for disease resistance genes. Transcriptomes of the plant-fungi interaction identified differentially expressed genes associated with virulence in *Rhizoctonia* and resistance in Tartary

buckwheat. Integration with jasmonate-mediated transcriptome and metabolome changes revealed a negative regulator of jasmonate signaling, cytochrome P450 (*FtCYP94C1*), as increasing disease resistance probably via accumulation of resistance-related flavonoids. The integration of resistance data for 320 Tartary buckwheat accessions identified a gene homologous to aspartic proteinase (*FtASP*), with peak expression following *R. solani* inoculation. FtASP exhibits no proteinase activity but functions as an antibacterial peptide that slows fungal growth. This work reveals a potential mechanism behind pathogen virulence and host resistance, which should accelerate the molecular breeding of resistant varieties in economically essential crops.

Key words: *Rhizoctonia solani*, comparative genomics, GWAS, virulence, resistance, Tartary buckwheat.

INTRODUCTION

Rhizoctonia solani, belonging to the phylum Basidiomycota, is an aggressive soil-borne hemibiotrophic pathogen causing devastating diseases worldwide in a wide range of economically important crops, such as rice (*Oryza sativa*), wheat (*Triticum aestivum*), maize (*Zea mays*), potato (*Solanum tuberosum*), soybean (*Glycine max*), tomato (*Solanum lycopersicum*), sugar beet (*Beta vulgaris*) and cabbage (*Brassica oleracea*) (Yang and Li, 2012). Plant defense against pathogen attack usually activates plant hormone signaling pathways involving jasmonic acid (JA), ethylene (ET) and salicylic acid (SA; Bari and Jones, 2009; Kouzai et al., 2018). However, the precise mechanism of action of phytohormones in plant disease resistance is yet to be fully uncovered. At present, the control of *R. solani* in fields is highly dependent on chemical fungicides, while cultural practices and biological control have little effect (Molla et al., 2020). Given these facts, the development of genetically encoded resistance has become an ideal alternative approach to combat the pathogen.

Omics (genomics, transcriptomics, proteomics and metabolomics) platforms have been used to understand pathogenesis and host defense in several studies. Draft genome sequences are available for different *R. solani* isolates representing four anastomosis groups (AGs), namely rice AG1-IA (Zheng et al., 2013), lettuce (*Lactuca sativa*) AG1-IB (Wibberg et al., 2013), sugar beet AG2-2IIIB (Wibberg et al., 2016), potato AG3-PT (Wibberg et al., 2017) and wheat AG8 (Hane et al., 2014). Comparative genomic and transcriptomic studies of *R. solani* isolates have revealed differences in their genetic structure and gene expression profiles that may contribute to the host preference and virulence of this pathogen (Xia et al., 2017; Lee et al., 2021; Mat Razali et al., 2021). Metabolite profiles of *R. solani*-infected rice demonstrated an alteration of the glycolytic and oxidative pentose phosphate pathways as well as of secondary

metabolism (Mutuku and Nose, 2012). Quantitative trait locus (QTL) analysis for rice sheath blight resistance has been well studied and summarized (Molla et al., 2020; Li et al., 2021). Recently, genes associated with sheath blight resistance were identified in maize (Li et al., 2019) and rice (Wang et al., 2021a) by a genome-wide association study (GWAS).

Multinucleate *R. solani* isolates are divided into 14 physiologically and genetically distinct anastomosis groups (AG-1 to AG-13, AGB1), some of which include several subgroups (Yang and Li, 2012). *R. solani* AG4-HGI 3 was isolated from Tartary buckwheat [*Fagopyrum tataricum* (L.) Gaertn.] and can cause stem canker, damp-off and death of seedlings, resulting in severe yield loss (Li et al., 2020). The genetic resistance of Tartary buckwheat against this disease, however, remains unknown. In this work, we report on the genome sequence of *R. solani* AG4-HGI 3 and performed a comparative analysis with the genomes of other *R. solani* isolates. We discovered a JA-induced response to *R. solani* in Tartary buckwheat when pathogen and host plants interact. Based on the evaluation of the response to *R. solani* in 320 Tartary buckwheat accessions, we used GWAS to identify loci associated with disease resistance. We identified the two candidate resistance genes cytochrome P450 (*FtCYP94C1*) and aspartic proteinase (*FtASP*) and functionally analyzed them here. The genetic resource presented in this work should contribute to the development of effective techniques for controlling this devastating pathogen.

RESULTS

Genome assembly identified abundant pathogenesis-related genes in *R. solani* AG4-HGI 3

To compare *R. solani* AG4-HGI 3 with other isolates, we explored candidate host crops of *R. solani* AG4-HGI 3. Inoculation experiments showed that the host range of *R. solani* AG4-HGI 3 is very extensive, as it infected not only the monocot plant species rice and wheat, but also species of Eudicots in the Brassicaceae, Cucurbitaceae, Leguminosae, Solanaceae, and Amaranthaceae families (cucumber [*Cucumis sativus*], lettuce, *Nicotiana benthamiana*, and tomato, among others; Supplemental Figure S1). The broad host range of *R. solani* AG4-HGI 3 piqued our interest to study the mechanism underlying pathogenicity in this isolate. Staining with DAPI (4′,6-diamidino-2-phenylindole) demonstrated that *R. solani* AG4-HGI 3 is a multinucleate

isolate, with the number of nuclei in a single cell varying (Supplemental Figure S2). We determined the genome sequence of *R. solani* AG4-HGI 3 using Illumina HiSeq and PacBio sequencing platforms (Supplemental Data Set S1). The estimated genome size is 46.05 Mb with a heterozygous rate of about 1.49% (Supplemental Data S2), which was higher than that of most other multi-nuclei isolates, including *R. solani* AG1-IA (0.12%, Zheng et al., 2013) and AG1-XN (0.26%, Li et al., 2021). The assembled genome size is approximately 65.36 Mb, which is somewhat larger than the estimated genome size and that of most other *R. solani* isolates (Supplemental Data Sets S2, S3; Supplemental Figure S3). Accordingly, *R. solani* AG4-HGI 3 is predicted to contain at least 30% more protein-coding genes than all other sequenced *R. solani* isolates (Supplemental Figure S4). However, the GC content (48.2%) was similar to that of other *R. solani* isolates. The scaffold N50 value is 568.8 kb, which is higher than that obtained from the assembled genomes of *R. solani* AG4 (Kaushik et al., 2022). We assessed the quality of the draft genome using the Benchmarking Universal Single-Copy Orthologs (BUSCO) and the Core Eukaryotic Gene Mapping Approach (CEGMA), with completeness scores of 94.1% and 95.97%, respectively, indicating the high quality of our genome assembly (Supplemental Data Set S4). Further, 30% of all genes appear to be duplicated according to the BUSCO analysis and randomly distributed on the scaffolds, which likely underlies the gene number expansion in this strain (Supplemental Figure S5).

We identified a total of 438.6 kb (0.67%) of the *R. solani* AG4-HGI 3 genome as repeat-containing, comprising 546 elements from 16 DNA transposons and retrotransposons families (Supplemental Data Set S5). These transposons are randomly distributed on the scaffolds (Supplemental Figure S5). The content of repeat elements varies across isolates (Supplemental Data Set S6) and the proportion of repeat elements is lower in AG4-HGI 3 than in other *R. solani* isolates (Zheng et al., 2013; Hane et al., 2014; Lee et al., 2021). The transposon element LTR-ERV1 (long terminal repeat-vertebrate retrovirus 1) appeared the most abundant, accounting for 0.13% of total repetitive element length. The numbers of DNA, long interspersed nuclear element (LINE), satellite and short interspersed nuclear element (SINE) transposons are modest compared to those from other isolates in *R. solani*, although some elements may have been missed in the more fragmented genomes of some isolates due to different sequencing and assembly strategies.

To investigate the phylogenetic relationships of all 23 *R. solani* available genomes in this work, we generated a maximum likelihood-based phylogenetic tree from single-copy orthogroups (Figure 1A). We determined that *R. solani* AG4-HGI 3 is closely related to the other AG4 strains, AG4-HGI 1 and AG4-HGI 2. Moreover, a syntenic analysis also identified a large number of syntenic relationships between *R. solani* AG4-HGI 3 with other AG4 strains (Supplemental Figure S6), confirming the close relationship between these strains. Genome comparison demonstrated that *R. solani* contains 9,630 orthogroups absent from *Magnaporthe oryzae* (Supplemental Data Set S7). Among them, 664 orthogroups were specific to *R. solani* AG4, of which 131 orthogroups are shared by the three isolates, and 350 orthogroups are specific to *R. solani* AG4-HGI 3 (Supplemental Data Set S8). We also identified 3,236 significantly expanded gene families (consisting of 11,339 genes) and 891 significantly contracted gene families (comprising 103 genes) ($P < 0.05$ computed with CAFÉ,) in *R. solani* AG4-HGI 3 (Figure 1A; Supplemental Figure S7; Supplemental Data Set S9). Of the 891 contracted gene families, 801 were apparently entirely absent in strain AG4-HGI 3. A gene ontology (GO) term enrichment analysis revealed that the expanded gene families are mainly enriched in catalytic activity and ion binding (Figure 1B). Of the genes in the expanded gene families, 394 were involved in glycosyl hydrolysis activity, and 74 were involved in pectate lyase activity. As the plant cell wall is mainly composed of cellulose, hemicellulose and pectin, and cell wall degradation are closely associated with the saprophytic lifestyle of fungi (Cantarel et al., 2009), the expansion of these cell wall degradation-related genes might be responsible for the broad host range of *R. solani* AG4-HGI 3.

Considering the broad host range of *R. solani* AG4-HGI 3, and given that the pathogenicity genes encoding carbohydrate-active enzymes (CAZymes), secreted proteins and effectors are prime weapons for pathogen infection and modulation of host morphology (Zheng et al., 2013; Kaushik et al., 2022), we turned our attention to these pathogenicity genes. CAZymes are necessary for phytopathogenic organisms to degrade the structural components of the cell wall and hence enter their host plants (Cantarel et al., 2009). We therefore characterized the CAZyme complement in *R. solani* and *M. oryzae*. We predicted a total of 1,026 CAZymes in *R. solani* AG4-HGI 3 (Supplemental Data Set S10; Supplemental Figure S5), accounting for 5.45% of all protein-coding genes, which was greater than in some isolates of *R. solani* (AG1-IA, AG1-IB-7/3/14, AG3-PT-1AP and AG8-WAC10335) and *M. oryzae* (Supplemental

Data Set S11). We identified a greater proportion of CAZymes involved in lignin, cellulose, hemicellulose and pectin degradation in *R. solani* AG4-HGI 3 compared to AG1-IA and AG8-WAC10335 (Figure 1A; Supplemental Data Set S12), which was in accordance with the expanded number of genes related to glycosyl hydrolysis and pectate lyase activity in *R. solani* AG4-HGI 3. Secreted proteins are essential in inhibiting the defense response of host cells (Lee et al., 2021): we predicted a total of 1,167 secreted proteins in *R. solani* AG4-HGI 3 (Supplemental Data Set S13), accounting for 6.20% of all protein-coding genes, which is relatively lower than in most other *R. solani* isolates (Supplemental Data Set S14). Moreover, we identified relatively fewer predicted effectors in AG4-HGI 3 (accounting for 1.56% of the protein-coding genes) relative to most other strains (Supplemental Data Sets S15 and S16). In addition, the proportion of CAZymes was higher in most *R. solani* strains compared to *M. oryzae*, while *R. solani* was characterized by a smaller proportion of secreted proteins and effectors than *M. oryzae*. These findings might be an important feature that distinguish this species from *M. oryzae*, and in accordance with previous work demonstrating fewer secreted proteins in *R. solani* than in other filamentous pathogens (Anderson et al., 2017). Moreover, we predicted 2,355 virulence genes, 3,099 pathogen-host interaction genes, 2,124 transporter genes, 2,071 transmembrane protein genes and 19 secondary metabolite biosynthesis gene clusters in *R. solani* AG4-HGI 3 (Supplemental Data Sets S17–S21). These candidate genes are randomly distributed across the scaffolds (Supplemental Figure S5), and represent a valuable resource to reveal the intimate mechanism of *R. solani* infection of susceptible plant species.

Upregulated pathogenesis-related genes are involved in *R. solani* AG4-HGI 3 infection of Tartary buckwheat

To gain insight into the pathogenesis of *R. solani* AG4-HGI 3 infection of Tartary buckwheat, we performed an RNA-seq analysis of *R. solani* AG4-HGI 3 at three infection stages (6 h, water-soaked spots appeared, 14 h, spots expansion significantly, and 22 h, rotten and necrotic spots appeared) using the assembled genome of *R. solani* AG4-HGI 3 as a reference (Supplemental Figure S9; Supplemental Data Set S22). The strain without host infection was used as negative control. In total, we determined that 19,140 genes (including 18,821 protein-coding genes, 265 transfer RNAs [tRNAs] and 54 ribosomal RNAs [rRNAs]) are expressed at some point during infection. Of these, 16.8% (3,215 out of 19,140) were upregulated in at least one time point and 270 genes were upregulated at all time points (Supplemental Data Set S23; Supplemental Figure

S10). Further, 503 genes were upregulated within the first 6 h of Tartary buckwheat infection by *R. solani* AG4-HGI 3 (Figure 2A), rising dramatically after infection for 14 h to 2,102 genes, while slightly increasing after 22 h of infection (2,655 genes), suggesting that the transcriptome of *R. solani* AG4-HGI 3 reacts strongly after 14 h of infection. We analyzed the functions of all 3,215 upregulated genes according to their annotation in the assembled genome. In total, 477 virulence genes, 401 genes encoding secreted proteins, 695 genes encoding pathogen-host interaction proteins and 107 genes encoding effectors were upregulated in at least one time point (Figure 2B; Supplemental Data Set S23). A Kyoto Encyclopedia of Genes and Genomes (KEGG) pathway enrichment analysis revealed that the highly expressed transcripts are significantly enriched in the ribosome (Figure 2C), suggesting that transcript translation is metabolically active during *R. solani* AG4-HGI 3 infection of Tartary buckwheat. The list of these upregulated pathogenesis-related genes will undoubtably provide further clues to reveal the mechanism during *R. solani* AG4-HGI 3 infection of Tartary buckwheat.

We also analyzed the expression level of expanded gene families in *R. solani* AG4-HGI during infection of Tartary buckwheat (Supplemental Data Sets S24-S27). Most (>70%) of the genes in expanded gene families exhibited no significant change during infection of Tartary buckwheat. Less than a quarter of expanded gene families exhibited more differentially expressed genes than unchanged genes. In addition, the proportions of upregulated and downregulated genes in expanded gene families were lower than that for the whole genome following infection for 6 h and 22 h, while we observed the opposite pattern 14 h into infection, further confirming that this time point is crucial for *R. solani* AG4-HGI 3 infection. Less than a quarter of expanded gene families exhibited larger proportions of upregulated or downregulated genes than that for the whole genome. We conducted GO and KEGG analyses to investigate the expression pattern of expanded gene families with specific functions (Supplemental Figures S11, S12). We observed that the upregulated expanded gene families are mainly enriched in genes related to pentose and glucuronate interconversion, cyanoamino acid metabolism, ribosome, starch and sucrose metabolism and cysteine and methionine metabolism. The downregulated expanded gene families were mainly enriched in genes related to glycolysis/gluconeogenesis, amino sugar and nucleotide sugar metabolism, methane metabolism, arginine and proline metabolism and ABC transporters.

As with expanded gene families, the expression level of most genes in contracted gene families exhibited no changes during infection of Tartary buckwheat (Supplemental Data Sets S28–S31). Less than 3% of contracted gene families had more differentially expressed genes than unchanged genes. In addition, the proportions of upregulated and downregulated genes in contracted gene families were higher than that for the whole genome. Less than 2.5% of contracted gene families exhibited larger proportion of upregulated or downregulated genes than that for the whole genome. GO and KEGG analyses revealed that the upregulated contracted gene families are mainly enriched in genes related to sulfur metabolism, carbon metabolism, lysine degradation, monobactam biosynthesis and riboflavin metabolism (Supplemental Figures S13, S14). The downregulated contracted gene families were mainly enriched in genes related to glycolysis/gluconeogenesis, pyruvate metabolism, glycerophospholipid metabolism and carbon metabolism. The varied gene number and expression level of these gene families with specific functions may help further reveal the infection mechanism of *R. solani* AG4-HGI 3.

As comparative genomics revealed that *R. solani* AG4-HGI 3 has more CAZyme genes than other *R. solani* isolates, we examined the expression levels of genes encoding CAZymes during *R. solani* AG4-HGI 3 infection of Tartary buckwheat in detail. Overall, nearly half (467 out of 1,026) of all genes encoding CAZymes were upregulated at at least one time point during Tartary buckwheat infection by *R. solani* (Supplemental Data Sets S32 and S33). Notably, 424 CAZyme genes were upregulated at 14 h into infection, which was more than at 6 h (76 genes) and 22 h (387 genes), suggesting that this period is important for the degradation of the cell wall of Tartary buckwheat by *R. solani*. Further analysis indicated that 106 of these upregulated CAZymes were involved in cellulose degradation, another 117 were involved in hemicellulose degradation, 174 in pectin degradation and 35 in lignin degradation (Figure 2D; Supplemental Data Set S34). Identification of these upregulated CAZyme genes will help reveal specific components of the plant cell wall degradation machinery during *R. solani* infection.

To investigate the mechanism of *R. solani* AG4-HGI 3 infection of Tartary buckwheat, we assessed the functions of virulence genes experimentally by transient heterologous expression in *Nicotiana benthamiana* leaves. We chose *YTH domain-containing protein* (*RsYTHDC*, gene04142), *proline-rich protein* (*RsPRP*, gene00437) and *laminin domain-containing protein* (*RsLDCP*, gene15409), which are homologs of

virulence genes (AG1IA_00579; AG1IA_04049 and AG1IA_06427) previously identified in *R. solani* AG1-IA (Zheng et al., 2013). *D-arabinitol 2-dehydrogenase* (*RsDAD*, gene08192) is a *R. solani* AG4-HGI 3 specific interacting virulence gene that is significantly upregulated during *R. solani* AG4-HGI 3 infection for 14 h and 22 h. We individually expressed *RsYTHDC*, *RsPRP*, *RsLDCP* and *RsDAD* from *R. solani* AG4-HGI 3 in *N. benthamiana* leaves (Supplemental Figure 15) and evaluated disease resistance following subculture with mycelial disks for 48 h. None these four virulence genes caused any morphological changes to the infiltrated leaves in normal growth conditions (Supplemental Figure S16), but significantly enhanced disease susceptibility compared to the control, as measured by relative fungal biomass and MDA content (Figure 2E; Supplemental Figures S17, S18), suggesting that these virulence genes might help pathogens infect host plants successfully.

To explore the function of these virulence proteins in plants, we determined the subcellular localization of RsYTHDC and RsDAD fused to the green fluorescent protein (GFP). A transient *N. benthamiana* expression assay indicated that RsYTHDC and RsDAD localize in both the cytoplasm and nucleus (Supplemental Figure S19), suggesting that these virulence factors may help pathogen infection by interacting with plant proteins. We also looked for proteins interacting with RsYTHDC or RsDAD using a combination of pull-down and mass spectrometry method (Supplemental Figure S20; Brymora et al., 2004). We obtained 236 and 192 candidate proteins that might interact with RsYTHDC or RsDAD, respectively (Supplemental Data Sets S35, S36). Most homologous of the candidate RsYTHDC-interacting proteins were previously described to confer disease resistance, including endochitinase (FtPinG0404899000) (Bai et al., 2021), aquaporin (FtPinG0606269900) (Tian et al., 2016), polygalacturonase-inhibiting protein (FtPinG0505912500 and FtPinG0707633000) (Borras-Hidalgo et al., 2012), UDP glycosyltransferase (FtPinG0707681200) (Pasquet et al., 2016; He et al., 2020), mitogen-activated protein kinase (FtPinG0505354900) (Wang et al., 2021b), oxalate-CoA ligase (FtPinG0201520900) (Peng et al., 2017), cationic peroxidase (FtPinG0606353800) (Wally and Punja, 2010), annexin (FtPinG0404585800) (Zhao et al., 2019), vacuolar-processing enzyme-like (FtPinG0303401000) (Wang et al., 2017; Dong et al., 2022) and protein THYLAKOID FORMATION1 (FtPinG0808541100) (Wangdi et al., 2010). Likewise, homologous of some candidate RsDAD-interacting proteins have been previously shown to enhance disease resistance: major latex protein (FtPinG0100209300) (Yang et al., 2015),

chorismate synthase (FtPinG0505432600) (Hu et al., 2009), peptide methionine sulfoxide reductase (FtPinG0100988800) (Oh et al., 2010), serine hydroxymethyltransferase (FtPinG0202435800) (Moreno et al., 2005), and L-ascorbate peroxidase (FtPinG0403764100) (Liu et al., 2018). Homologous of other putative interactors with RsDAD included disease susceptibility genes encoding nucleoside diphosphate kinase (FtPinG0707189500 and FtPinG0808916000) (Ye et al., 2020), isocitrate dehydrogenase (FtPinG0505344500) (Mhamdi et al., 2010), monodehydroascorbate reductase (FtPinG0404369900) (Feng et al., 2014), ferredoxin-dependent glutamate synthase (FtPinG0707851300) (Chen et al., 2016) and phosphate transporter (FtPinG0707291400) (Dong et al., 2019). We employed bimolecular fluorescence complementation (BiFC) assays to verify the interaction between the virulence proteins and their candidate interacting proteins. We established that a serine hydroxymethyltransferase (FtSHMT, FtPinG0202435800) can interact with the virulence protein RsDAD, suggesting the reliability of these candidate interacting proteins (Supplemental Figure S21). However, as the function of their encoding genes in Tartary buckwheat response to *R. solani* AG4-HGI 3 infection might be varied, further study is needed to ascertain the function of these candidate interacting proteins.

JA is involved in Tartary buckwheat resistance to *R. solani* AG4-HGI 3

Although the study of the fungal genome and the plant-fungus interaction transcriptome can help us understand the pathogenesis of the strains, how plants respond to these fungal infections remains unclear. Through studying the mechanism of host plant response to pathogens, exploitation and utilization of disease resistance genes represent an important means to improve the disease resistance of host plants. To better understand the host plant response to *R. solani*, we analyzed the transcriptomes of Tartary buckwheat in response to *R. solani* AG4-HGI 3 infection (Supplemental Data Set S37). In total, 48.5% (17,745 out of 36,613) of Tartary buckwheat genes were differentially expressed in at least one time point during *R. solani* AG4-HGI 3 infection (Supplemental Data Set S38; Supplemental Figure S22). Again, the number of differentially expressed genes peaked at 14 h (14,698 genes) and 22 h (15,200 genes), nearly twice as many as at 6 h (7,773 genes), suggesting that the Tartary buckwheat transcriptomic response to infection is greatest when the pathogen is most active. A KEGG analysis revealed that a large fraction of differentially expressed genes is involved in plant secondary metabolite biosynthesis, as well as phytohormone signaling

(Figure 3A), suggesting that these pathways are of critical importance to the plant response to *R. solani* infection.

We investigated the function of disease-related phytohormones on plant defense against *R. solani*, by evaluating disease resistance of Tartary buckwheat seedlings pre-treated with the phytohormones gibberellin (GA), ethylene (ET), salicylic acid (SA) and jasmonate acid (JA; Supplemental Figure S23). We observed that the sunken lesion and dark brown symptoms are visibly alleviated in Tartary buckwheat seedlings pre-treated with JA, but not with other phytohormones, compared to the control pre-treated with DMSO. We thus speculated that JA might play an important role in Tartary buckwheat defense against *R. solani* AG4-HGI 3 infection. As JA is a plant hormone that plays important roles in the regulation of plant secondary metabolites biosynthesis and disease resistance (Bari and Jones, 2009; De Geyter et al., 2012; Verma et al., 2016; Zhou and Memelink, 2016), we focused on the expression level of genes involved in JA biosynthesis and signaling. In total, 62 differentially expressed genes appeared involved in JA biosynthesis and signaling (Figure 3B; Supplemental Data Set S39), suggesting that JA signal transduction plays an important role during *R. solani* infection of Tartary buckwheat.

As numerous JA signaling genes were differentially expressed during *R. solani* infection, we studied the involvement of JA signaling during host plant response to *R. solani* infection. To this end, we determined the kinetic response of the transcriptome following methyl jasmonate (MeJA) treatment at different time intervals (1 h, 4 h and 12 h; *i.e.*, the early stages of infection where the greatest responses are seen by both the pathogen and the plant; Supplemental Data Set S40). We identified the Tartary buckwheat genes that are differentially expressed during *R. solani* infection and following MeJA treatment. We established that 29.3% (5,205 out of 17,745) of the genes differentially expressed during *R. solani* infection are also differentially expressed following MeJA treatment (Figure 3C; Supplemental Data Set S41; Supplemental Figure S24), confirming that JA signaling plays an essential role in Tartary buckwheat response to *R. solani*. A KEGG analysis revealed that many differentially expressed genes are involved in phenylpropanoid and flavonoid biosynthesis (Figure 3D). As previous research has shown that JA can regulate flavonoid biosynthesis (Zhou et al., 2017; Zhang et al., 2018; Chen et al., 2019; Ding et al., 2021), and flavonoids are involved in biotic stress responses (Misra et al., 2010;

Ullah et al., 2017), we speculated that JA might regulate flavonoids biosynthesis, hence modulating the disease resistance of Tartary buckwheat.

Of the above genes significantly upregulated during *R. solani* infection and MeJA treatment, we characterized the JA signaling transduction gene *FtCYP94C1* (FtPinG0808388800), homologous to Arabidopsis *CYP94C1*, encoding an enzyme responsible for JA-Ile oxidation to 12OH-JA-Ile (Heitz et al., 2012) (Figure 4A–C). Heterologous expression of *FtCYP94C1* in Arabidopsis or its overexpression in Tartary buckwheat exhibited no change in phenotype compared to wild-type plants, while resulting in significantly enhanced disease resistance compared to the controls (Figure 4D, 4E and Supplemental Figures S25–S28), as also described in its homolog gene in Arabidopsis (Poudel et al., 2019). Various JA biosynthesis and signaling mutants (*aoc4*, *jar1* [*jasmonate resistant 1*] and *myc2 myc3 myc4*) displayed decreased disease resistance compared to the controls (Supplemental Figures S29–S31), and pretreatment with JA increased their disease resistance index, suggesting a positive role for JA signaling on plant defense against *R. solani* AG4-HGI 3. However, the disease resistance ability of *FtCYP94C1* was in contrast with the well-known reduced capacity of 12OH-JA-Ile in promoting the formation of the COI1–JAZ (CORONATINE INSENSITIVE 1– JASMONATE-ZIM-DOMAIN PROTEIN 1) receptor complex (Koo et al., 2011; Heitz et al., 2012; Koo et al., 2014), and the positive regulation disease resistance by JA signaling (Verma et al., 2016; Pan et al., 2020), suggesting that *FtCYP94C1* may regulate Tartary buckwheat resistance to *R. solani* through other pathways beside typical JA signaling. As many genes differentially expressed during both *R. solani* infection and MeJA treatment were involved in flavonoid biosynthesis, and the positive regulation of 12OH-JA-Ile in flavonoid biosynthesis (Poudel et al., 2019), we analyzed the metabolome of *FtCYP94C1* overexpression Arabidopsis lines to investigate the metabolic changes involved in disease resistance (Supplemental Figure S32; Supplemental Data Set S42). 12OH-JA-Ile significantly accumulated in *FtCYP94C1* overexpression lines, confirming that FtCYP94C1 is responsible for JA-Ile oxidation to 12OH-JA-Ile. Moreover, the flavonoids including rutin, quercitrin and chalcone also accumulated in *FtCYP94C1* overexpression lines (Figure 4F). Flavonoid contents significantly decreased in JA biosynthesis and signaling mutants (*aoc4*, *jar1* and *myc2 myc3 myc4*; Supplemental Figure S33), and significantly increased after JA treatment, suggesting a positive role for typical JA signaling on flavonoid content. As flavonoids have been previously reported to enhance disease resistance (Yamamoto et

al., 2000; Misra et al., 2010; Yang et al., 2016; Schenke et al., 2019), we speculate that FtCYP94C1 may not function through the typical JA signaling pathway by promoting the formation of COI1-JAZ receptor complex, but rather by increasing the accumulation of disease resistance-related flavonoids.

We noticed that the expression of genes encoding some of the candidate proteins interacting with the virulence proteins RsYTHDC and RsDAD respond to both *R. solani* infection and MeJA treatment. Among them, homologous of UDP-glycosyltransferase (FtPinG0707681200) is involved in the biosynthesis of plant disease-related secondary metabolites (Pasquet et al., 2016; He et al., 2020). Homologous of polygalacturonase-inhibiting proteins (FtPinG0505912500 and FtPinG0707633000) are structural glycoproteins of the plant cell wall with antifungal activity; they can specifically bind to and inhibit fungal polygalacturonases (Ferrari et al., 2003). The expression of these disease resistance genes was mostly upregulated after both *R. solani* infection and MeJA treatment (Supplemental Data Sets S35 and S36), as previously reported in Arabidopsis and golden root (*Rhodiola sachalinensis*) (Ferrari et al., 2003; Yu et al., 2011). The possible interaction between virulence proteins and these disease resistance proteins may result in the disfunction of resistance proteins, hence reducing the plant immune response and help pathogens infect their host successfully. We speculate that the JA-induced expression of these disease resistance genes may alleviate the disfunction of their encoded resistance proteins, thus helping Tartary buckwheat better resist pathogen infection. However, this conjecture needs to be tested.

Integrating GWAS and gene expression data to accurately identify candidate genes that confer resistance to *R. solani* AG4-HGI 3 in Tartary buckwheat

Although the JA signaling pathway gene *FtCYP94C1* was demonstrated above to be connected to Tartary buckwheat resistant to *R. solani* AG4-HGI 3, the functions of many other Tartary buckwheat genes differentially expressed during both *R. solani* infection and MeJA treatment remain unknown. Moreover, their involvement in disease resistance needs to be elucidated. In particular, it is necessary to find a suitable method to narrow down the number of candidate disease resistance genes. We thus turned to GWAS in combination with transcriptome analysis to mine for disease resistance genes. To this end, we measured the disease index of 320 Tartary buckwheat accessions collected worldwide (Supplemental Data Set S43). The coefficient of variation (CV) was approximately 65.6%, indicating that disease resistance is highly variable among

Tartary buckwheat varieties, providing valuable genetic resources for cultivating varieties with high disease resistance. Then, using polymorphisms identified in our previous efforts to sequence the genome of these varieties (Zhang et al., 2021), we carried out GWAS to identify genomic regions significantly associated with *R. solani* resistance, using the disease index as phenotype (Supplemental Figure S34). We identified a total of 122 significant single nucleotide polymorphisms (SNPs) located on 7 out of the 8 chromosomes. We looked for candidate genes in 200 kb of flanking sequences on either side near each significant SNP, resulting in 16 genomic regions harboring 790 genes (Figure 5A; Supplemental Data Set S44).

A KEGG analysis revealed that 14 candidate genes are involved in plant-pathogen interactions, confirming the reliability of the GWAS results (Supplemental Figure S35). Among them, homologous of WRKY transcription factor gene (FtPinG0809055500) are important regulator of plant defense responses (Pandey and Somssich, 2009). *3-ketoacyl-CoA synthase* (FtPinG0708058700) is a wax biosynthesis gene whose Arabidopsis homolog was shown to be involved in disease resistance (Weidenbach et al., 2014; Zhang et al., 2019b; Wang et al., 2019b). Homologous of LysM domain receptor-like kinase (FtPinG0100600300) are necessary in plant recognition of the fungal cell wall major component chitin (Wan et al., 2012; Ao et al., 2014; Paparella et al., 2014). Homologous of calcium-dependent protein kinase (FtPinG0100542000; Bundo and Coca, 2016; Wei et al., 2016; Bundó and Coca, 2017; Lu et al., 2020; Wu et al., 2021) are positive, while homologous of cyclic nucleotide-gated ion channel (FtPinG0100588800; Moeder et al., 2011; Wang et al., 2019a) are negative regulators of disease resistance. The identification of these plant-pathogen interaction-related genes confirm the reliability of the GWAS results, and provide important clues for understanding the genetic architecture of disease resistance in Tartary buckwheat. In addition, as plant disease resistance is tightly associated with the content of secondary metabolites, which is greatly affected by the environment, we compared the above GWAS regions with our previous metabolic GWAS (mGWAS) data (Zhao et al., 2022). We observed an overlap between five regions associated with three disease resistance metabolites and disease index (Supplemental Data Set S45; Supplemental Figure S36). The metabolites tangeretin (Liang et al., 2021), indole (Shen et al., 2018) and indole-3-carboxylic acid (Gamir et al., 2012; Pastor-Fernández et al., 2019) have been previously shown to be involved in plant disease resistance.

We integrated all GWAS results with the transcriptomes from *R. solani* inoculation and JA treatment to screen candidate disease resistance genes. We detected 106 genes located in 15 associated regions whose transcript levels respond to both *R. solani* infection and MeJA treatment (Figure 5B; Supplemental Data Set S46). Among them, 49 genes were upregulated during *R. solani* infection and MeJA treatment. Most of these genes have been previously shown increased the plant disease resistance in other plant species, including homologous of *aspartic proteinase* (*FtASP*, FtPinG0302743900; Xia et al., 2004; Prasad et al., 2009), *alcohol dehydrogenase* (*FtADH1*, FtPinG0302737400; Shi et al., 2017), *calcium-dependent protein kinase* (FtPinG0100542000; Bundo and Coca, 2016; Wei et al., 2016; Bundó and Coca, 2017; Lu et al., 2020; Wu et al., 2021), *BTB/POZ domain-containing protein* (FtPinG0607121100; Zhang et al., 2019a), *cellulose synthase* (*FtCSLG2*, FtPinG0404615400; Choe et al., 2021) and *carboxylesterase* (*FtCES18*, FtPinG0809058900; Ko et al., 2016). The upregulation of these JA-induced genes during *R. solani* infection might contribute to JA-induced disease resistance responses. Sixteen genes were downregulated during *R. solani* infection, while upregulated after MeJA treatment. Most of these genes were previously shown have disease resistance ability in other plant species, including homologous of an ABC transporter gene (FtPinG0404610000; Bienert et al., 2012; Sasse et al., 2016; Khare et al., 2017), *E3 ubiquitin-protein ligase* (FtPinG0404612300; Karki et al., 2021), *ferredoxin* (FtPinG0707939600; Huang et al., 2007; Ger et al., 2014; Wang et al., 2018; Cui et al., 2021) and *glutamate receptor* (FtPinG0708049000; Liu et al., 2021). The downregulation of these JA-induced resistance genes during *R. solani* infection might be necessary for pathogens to infect plant cells successfully. In summary, the majority of the overlapping genes obtained by GWAS and transcriptomics were related to disease resistance, suggesting that the combination of GWAS with transcriptome data can be an effective strategy for screening candidate disease resistance genes.

JA-induced *FtASP* inhibits *R. solani* AG4-HGI 3 infection by suppressing fungal growth

To clarify the functions of candidate disease resistance genes, and verify the efficiency of our strategy combining GWAS with transcriptomes in disease resistance gene screening, we chose candidate genes for experimental exploration: five genes identified by GWAS (*FtASP*, *FtADH1*, *FtPG1*, *FtCES18*, *FtCSLG2*) that are significantly upregulated during *R. solani* infection and following MeJA treatment; one

gene identified by GWAS (*FtKCS11*) that is significantly downregulated during *R. solani* infection but is upregulated following MeJA treatment (Figure 5B). We heterologously expressed all genes individually in Arabidopsis and subjected their leaves to disease resistance assays (Supplemental Figure S37). Five genes (*FtASP*, *FtADH1*, *FtPG1*, *FtCES18* and *FtKCS11*) resulted in enhanced disease resistance (Figure 6, Supplemental Figures S38 and S39). One gene (*FtCSLG2*) showed suppressed disease resistance (Supplemental Figures S38 and S39). Therefore, all genes tested in this assay changed plant disease resistance, confirming the high efficiency of our strategy combining GWAS with plant-pathogen interaction and phytohormone-related transcriptomes for exploitation of disease resistance genes.

It is worth noting that FtPinG0302743900, encoding an aspartic protease (FtASP), one of the candidate proteins interacting with the virulence protein RsYTHDC, showed highest expression during *R. solani* inoculation and was significantly upregulated following MeJA treatment, and was also identified by GWAS. Haplotype analysis indicated that the 320 Tartary buckwheat accessions can be divided into two main haplotypes for this gene, with the C-haplotype exhibiting a higher disease resistance than the T-haplotype (Figure 6A). Accessions with the C-haplotype were widely distributed, while those harboring the T-haplotype were mainly distributed in northern China (Supplemental Figure S40). RT-qPCR analysis determined that *FtASP* expression is negatively correlated with the disease index in different Tartary buckwheat accessions, confirming the disease resistance ability of *FtASP* (Figure 6B). The heterologous expression of *FtASP* in Arabidopsis had no effect on naïve plants, but significantly improved their resistance to *R. solani* AG4-HGI 3 (Figure 6D and 6E; Supplemental Figures S41-S43). Moreover, the addition of recombinant purified full-length FtASP and its first half (Supplemental Figure S44) inhibited the growth of *R. solani* AG4-HGI 3, while the addition of the second half of FtASP did not affect fungal growth (Figure 6F; Supplemental Figure S45). Previous work had indicated that aspartic proteases are involved in plant resistance to both bacterial and fungal pathogens (Xia et al., 2004; Prasad et al., 2009; Wang et al., 2022). We therefore speculate that *FtAPS* is a vital component of resistance to *R. solani* in Tartary buckwheat, and potentially other pathogens. However, a protease assay revealed that FtASP has no protease activity (Supplemental Figure S46); rather, the N-terminal protein sequence GTPLKFNTTLLSINKVGSGGTTI (amino acids 57-79) showed a high probability to

be an antimicrobial peptide (Waghu and Idicula-Thomas, 2019), suggesting that FtASP might not function as a protease, but as an antimicrobial peptide.

DISCUSSION

Rhizoctonia solani is a destructive and widespread fungal pathogen with significant scientific and economic importance (Dean et al., 2012). A better understanding of its pathogenicity is critical to develop effective disease resistance strategies. Isolates from some *R. solani* anastomosis groups (AG3, AG5 and AG8) exhibit a limited host range, while those in AG1 and AG2 can infect a broader spectrum of host plants (Wibberg et al., 2013). The universality and complexity of host range present great challenges for the study of the mechanisms underlying pathogenicity. At present, due to its economic importance, most research has concentrated on *R. solani* AG1-IA, the predominant causal agent of rice sheath blight disease, while the basis of pathogenicity of other isolates that infect other economically important crops has yet to be studied. Here, we demonstrated that a *R. solani* AG4 isolate (AG4-HGI 3), originally identified from Tartary buckwheat, could infect an extensive range of host plants, including plants in the Poaceae, Brassicaceae and Leguminosae, representing a similar host range to that determined for AG1 (Wibberg et al., 2013). To investigate the genetic basis of its wide range of host plants, we sequenced and assembled the genome of *R. solani* AG4-HGI 3. Notably, we established that *R. solani* AG4-HGI 3 was a multi-nucleus isolate, with a variable number of nuclei number in a single cell. The specificities of this isolate bring great difficulties to genome assembly, resulting in the inability to reach chromosome-level scaffolding (Hane et al., 2014; Duan et al., 2022). The assembled genome of *R. solani* AG4-HGI 3 was larger than that of other *R. solani* isolates, which might be also due to the higher number of nuclei within a single cell (Takashima et al., 2018). Comparative genomic analysis showed that *R. solani* AG4-HGI 3 possessed abundant carbohydrate degradation-related genes and secreted proteins encoding genes, which might be associated with its extensive host range. Transcriptome analysis revealed that the expression of numerous genes in *R. solani* increased following 14 h of infection, with nearly half of CAZyme genes being upregulated at this time point, suggesting that this period may be necessary for *R. solani* AG4-HGI 3 infection and plant cell wall degradation. Similar results were previously obtained following infection of rice with *R. solani* AG1-IA, with most genes being differentially expressed at 18 h post inoculation (Zheng et al., 2013). In addition,

abundant pathogenesis-related genes were upregulated during *R. solani* infection, including some encoding key effectors previously identified as essential for *R. solani* pathogenesis such as proteins with NUDIX, NACHT or BTB domains (Li et al., 2021). Our findings therefore add to the knowledge necessary to help reveal the genetic and biological mechanisms during *R. solani* pathogenicity.

Previous research indicated that genes involved in plant hormone signaling are differentially expressed during *R. solani* infection (Zrenner et al., 2021) and elevating JA levels enhanced rice resistance against *R. solani* (Taheri et al., 2010). However, how JA participates in the regulation of plant disease resistance has yet to be fully uncovered. Here, we identified numerous JA-induced genes as being involved in the Tartary buckwheat response to *R. solani* infection. Among them, *FtCYP94C1* was a negative regulator of the typical JA signaling pathway (Koo et al., 2011; Heitz et al., 2012; Koo et al., 2014), while a positive modulator of disease resistance-related flavonoid biosynthesis (Poudel et al., 2019). Combined with the enhanced disease resistance and metabolomic alterations of Arabidopsis lines heterologously expressing this gene, we suggest that *FtCYP94C1* enhances disease resistance of Tartary buckwheat by regulating flavonoid biosynthesis rather than via the typical JA signaling pathway. In addition, we detected several JA-induced genes that were involved in Tartary buckwheat disease resistance. However, due to the complexity of plant disease, there is no universal relationship between classes of genes and pathogen resistance. For instance, some aspartic proteases (Xia et al., 2004; Prasad et al., 2009), cellulose synthases (Choe et al., 2021), alcohol dehydrogenases (Shi et al., 2017) and carboxylesterases (Ko et al., 2016) enhance disease resistance, while others suppress disease resistance (Hernández-Blanco et al., 2007; Liu et al., 2014; Wang et al., 2022). Here, we showed that the protease-like protein FtASP exhibited no aspartic protease activity, although it did inhibit fungal growth through the activity of its N-terminal region. As some N-terminal peptides were found to exert antibacterial function and exhibit a wide spectrum of antimicrobial activity (Zhao et al., 2020), we speculate that FtASP may function as an antimicrobial peptide to inhibit *R. solani* growth. In summary, the exploration of these plant defense-related genes will enrich our understanding of how plant hormones regulate plant disease resistance, with implications for accelerating the molecular breeding of disease-resistant varieties of economically important crop species.

The exploitation of genetic variation in natural population via GWAS is an effective strategy for the identification of disease resistance genes (Kankanala et al., 2019; Molla et al., 2020). However, insufficient marker density, linkage disequilibrium and high false positive rates represent a severe challenge for functional validation of candidate resistance genes (Shu et al., 2021). The combination of GWAS and transcriptome analysis, as employed here, can overcome these limitations, and hence accurately identify critical candidate resistance genes. Although the integration of GWAS and transcriptome analysis has been used to identify disease resistance genes in the past (Wen et al., 2018; Yao et al., 2020; Shu et al., 2021), most of these studies only explored comparisons between the transcriptomes of resistant and susceptible plants. As large-scale transcriptome data are only available in a few major crops, some well-developed systematically analysis methods (such as summary data–based Mendelian randomization, SMR, Zhu et al., 2016) could not be widely used to integrate GWAS and RNA-seq data. Here, by combining the results from *R. solani* inoculation and JA-mediated transcriptome analyses, we determined that the JA signaling gene *FtCYP94C1* enhanced resistance to *R. solani* AG4-HGI 3 in Tartary buckwheat apparently by promoting the biosynthesis of disease resistance-related flavonoids. By combining transcriptomes obtained during the plant-pathogen interaction and following JA treatment with GWAS, we identified 106 candidate genes that may be associated with disease resistance, which we argue is an efficient approach to greatly reduce the number of candidate genes identified through each separate analysis and likely reduces the false positive identification of candidate resistance genes. In conclusion, our strategy efficiently identified key components of the *R. solani* pathogenicity response in Tartary buckwheat, which can be investigated in other crops susceptible to this strain with broad host range. Further, multi-omics analysis such as that presented in this work will enhance the understanding of pathogenicity of other diseases in other agronomically important crop species, thus streamlining the identification of candidate resistance genes for molecular breeding of disease resistance.

In summary, our study demonstrated that *R. solani* AG4-HGI 3 exhibited a larger genome size and harbored more protein-coding genes than most other *R. solani* isolates. Moreover, the expansion of pathogenicity genes might be responsible for the broad host range of *R. solani* AG4-HGI 3. In addition, some jasmonate-induced genes in Tartary buckwheat enhanced the resistance to *R. solani*. These results will enrich the knowledge

of pathogenicity in *R. solani*, and hence accelerate the molecular breeding of resistant varieties in economically important crops.

METHODS

Rhizoctonia solani AG4-HGI 3 isolates and culture conditions

The strain *R. solani* AG4-HGI 3 was isolated from Tartary buckwheat [*Fagopyrum tataricum* (L.) Gaertn.] in the field and characterized as AG4-HGI 3 (Li et al., 2020). This fungal isolate causes sunken lesions and dark brown symptoms on the root and stem of Tartary buckwheat. The cultures of *R. solani* AG4-HGI 3 were revived from stock cultures maintained at –80℃ by placing mycelial disks on fresh potato dextrose agar (PDA) for 5 days, at 28℃, in the dark. The isolates were then sub-cultured on fresh PDA for 5 days or potato dextrose broth (PDB) for 3 days, at 28℃, in the dark before being used for experiments. Nuclei in hyphae were stained using 4',6-diamidino-2-phenylindole (DAPI) according to the method described previously (Li et al., 2021).

Genome assembly and comparative genomics

The pathogen sub-cultured on PDB medium was used to extract the genomic DNA via a Fungal DNA Kit (D3390-02, Omega BioTek, Norcross, USA), according to the manufacturer's instructions. Purified DNA was quantified on a TBS-380 fluorometer (Turner BioSystems Inc., Sunnyvale, CA). The genome was sequenced using PacBio Sequel Single Molecule Real Time (SMRT) and Illumina sequencing platforms at Shanghai Majorbio Biopharm Biotechnology Co., Ltd., China. The genome size and heterozygosity of *R. solani* AG4-HGI 3 were estimated based on the distribution of 17-mers using Meryl (Rhie et al., 2020) and GenomeScope v1.0 (https://github.com/schatzlab/genomescope; Vurture et al., 2017). The Illumina short reads were quality-controlled using fastp v0.23.0 (https://github.com/OpenGene/fastp; Chen et al., 2018). The PacBio long reads were assembled using CANU v1.7 (http://canu.readthedocs.io/en/latest/; Koren et al., 2017). The assembled contigs were corrected and polished through Illumina short reads using RACON (https://github.com/lbcb-sci/racon; Vaser et al., 2017). For annotation, the open reading frames (ORFs) of genes were predicted using Maker 2 v2.31.9 (http://www.yandell-lab.org/software/maker.html; Cantarel et al., 2008) and annotated through alignment against the NR, Swiss-Prot, Pfam, GO, COG and KEGG databases using the sequence alignment tools BLAST, Diamond v0.8.35 (https://github.com/bbuchfink/diamond; Buchfink et al., 2015) and HMMER v3.1b2 (http://www.hmmer.org/; Eddy et al.,

1998). The rRNA and tRNA in the genome were predicted using Barrnap 0.4.2 (https://github.com/tseemann/barrnap/; Seemann, 2014) and tRNAscan-SE v 1.3.1 (http://lowelab.ucsc.edu/tRNAscan-SE/; Lowe and Eddy, 1997). Repeat regions were masked using RepeatMasker v4.0.7 (http://www.repeatmasker.org/RepeatMasker/; Tarailo-Graovac et al., 2009). Predicted secreted proteins were defined as proteins with a signal peptide using SignalP v5.0 (https://services.healthtech.dtu.dk/service.php?SignalP-5.0; Armenteros et al., 2019) and no transmembrane domains using TMHMM v2.0 (https://services.healthtech.dtu.dk/service.php?TMHMM-2.0). CAZymes were identified by applying dbCAN2 (https://bcb.unl.edu/dbCAN2/; Zhang et al., 2018). The Pathogen Host Interaction database (PHI-base, http://www.phi-base.org; Winnenburg et al., 2006) was used to find sequence homology relative to known virulence and pathogenicity markers. The effector proteins were predicted using effectorP v3.0 (https://effectorp.csiro.au; Sperschneider et al., 2022).

OrthoMCL v1.4 (http://www.orthomcl.org; Li et al., 2003) was used to construct orthologous gene families. MUSCLE v3.7 (http://drive5.com/muscle; Edgar et al., 2004) was used to align single-copy orthologous genes. RAxML v8.0.19 (https://cme.h-its.org/exelixis/web/software/raxml; Stamatakis et al., 2014) was used to construct the maximum likelihood-based phylogenetic tree by employing sequence alignments with *Magnaporthe oryzae* as the outgroup. The unfiltered alignment and phylogenetic tree of are provided as Supplemental Files 1 and 2. CAFÉ v1.6 (https://sourceforge.net/projects/cafehahnlab) was used to determine the expansion and contraction of orthologous gene families. Synteny was analyzed using MUMmer v3 (https://mummer.sourceforge.net/; Kurtz et al., 2004) and the Circos plot was drawn using ShinyCircos (https://github.com/YaoLab-Bioinfo/shinyCircos; Yu et al., 2018). Genes were annotated with GO annotation using InterProScan v5.53-87.0 (http://www.ebi.ac.uk/interpro/search/sequence/; Jones et al., 2014).

Transcriptome analysis

The surface-sterilized Tartary buckwheat seeds were grown for 21 days at 22℃ (day/night) under long-day conditions (16-h light/8-h dark). For the transcriptome analysis of the *R. solani*-Tartary buckwheat interaction, mycelial disks sub-cultured on PDA medium were used to infect the leaves of Tartary buckwheat (Chuanqiao 1#) seedlings for 6 h, 14 h and 22 h. For MeJA treatment, leaves of Tartary buckwheat seedlings were treated with 50 μM MeJA (W341002, Sigma-Aldrich, Taufkirchen,

Germany) for 1 h, 4 h or 12 h. Three independent biological replicates for each treatment were conducted. Each replicate was obtained by pooling samples from ten seedlings. Tartary buckwheat leaves were flash-frozen in liquid nitrogen and ground to a fine powder. Total RNA was extracted with TRIzol reagent (15596026, Invitrogen, Carlsbad, USA); genomic DNA was removed using DNase I (2270A, TaKara, Kusatsu, Japan). RNA-seq sequencing libraries were prepared using a TruSeq^{TM} RNA sample preparation Kit (RS-122-2001) from Illumina (San Diego, USA), and sequenced with an Illumina HiSeq X Ten/Nova Seq 6000 instrument. Raw paired-end reads were trimmed and quality-controlled by SeqPrep (https://github.com/jstjohn/SeqPrep) and Sickle (https://github.com/najoshi/sickle) with default parameters. Then, the clean reads were aligned to the reference genome of *R. solani* AG4-HGI 3 and Tartary buckwheat (HERA) with orientation mode using HISAT2 (http://ccb.jhu.edu/software/hisat2/index.shtml) software (Kim et al., 2015), respectively. The mapped reads for each sample were assembled by StringTie (http://ccb.jhu.edu/software/stringtie/index.shtml?t=example) in a reference-based approach (Pertea et al., 2015). The expression level of each transcript was calculated according to the fragments per kilobase of transcript per million fragments mapped (FPKM) method using RSEM (http://deweylab.biostat.wisc.edu/rsem/; Li et al., 2011). Differential expression analysis was performed using DESeq2 (Love et al., 2014), DEGseq (Wang et al., 2010) and EdgeR (Robinson et al., 2010). Genes with adjusted *P*-value ≤ 0.05 (corrected using the Benjamini-Hochberg method) and fold-change >2 or < 0.5 (compared to DMSO treatment for MeJA treatment and compared to non-inoculated control samples for *R. solani* infection) were considered to be significantly differentially expressed genes. Functional enrichment of these differentially expressed genes was analyzed using the GO and KEGG databases.

Recombinant protein purification and protease activity assay

Full-length cDNAs of *RsYTHDC*, *RsDAD*, *FtASP*, *FtASP-N* and *FtASP-C* were amplified and inserted into the pET-28a expression vector. Recombinant proteins were produced in *E. coli* BL21 (DE3) cells (CD601-02, TransGen, Beijing, China) with 0.1 mM isopropyl-D-1-thiogalactopyranoside (IPTG, I6758, Sigma-Aldrich, Taufkirchen, Germany) at 28℃ for 12 h. After sonication (200W, 0℃, 30 min; ultrasound for 5 s every 10 s), the crude extracts were centrifugated at 12,000 g for 10 min, at 4℃. Each supernatant was then purified using Ni-NTA Agarose (30210, Qiagen, Hilden, Germany). Immunoblotting of His-RsYTHDC, His-RsDAD and His-FtASP was

performed with anti-His (1:2000; CW0286, CWBIO, Beijing, China) antibody. The molecular weight was marked using Rainbow Prestained Broad Molecular Weight Protein Marker (RTD6106, Real-Times Biotechnology Co. Ltd, Beijing, China). Protease activity was assessed using an EnzChek Protease Assay Kit (E6639, Invitrogen, Carlsbad, USA) following the manufacturer's instructions. The Endoproteinase Asp-N sequencing grade (ENDOARGS-RO, Roche Diagnostics Gmbh, Mannheim, Germany) was used as a positive control. Three biological replicates were conducted and the experiments were performed three times. Primer sequences are listed in Supplemental Data Set S47. The antimicrobial peptide was predicted using CAMP (www.camp.bicnirrh.res.in; Waghu and Idicula-Thomas, 2020).

Subcellular localization of RsYTHDC and RsDAD

Full-length cDNAs of *RsYTHDC* and *RsDAD* were amplified and inserted into the pCAMBIA1300-GFP vector. p2300-35s-H2B-mCherry was used as a nuclear marker. The plasmid was transferred into *N. benthamiana* leaves using Agrobacterium (*Agrobacterium tumefaciens*) strain GV3101-mediated transient infiltration (Wang et al., 2023). Subcellular localization was observed using a laser scanning confocal microscope (Zeiss LSM900) with the wavelengths of 488 (excitation)/500–530 nm (emission) for GFP, and 561 (excitation)/590–640 nm (emission) for mCherry. Primer sequences are listed in Supplemental Data Set S47.

Pull-down experiments and mass spectrometry

Pull-down and mass spectrometry assays were performed as described with some modifications (Brymora et al., 2004). Recombinant His-RsYTHDC and His-RsDAD proteins were used as bait. Total protein from Tartary buckwheat seedling was used as prey. The bait proteins were mixed with soluble protein extracts from Tartary buckwheat seedlings for 2 h at 4°C, and then immobilized on a Ni-NTA agarose (30210, Qiagen, Hilden, Germany). Weakly bound proteins were removed by washing three times with wash buffer (10 mM phosphate buffered saline [PBS pH 8.0, 20 mM imidazole, 0.005% [v/v] Tween 20). After elution with elution buffer (10 mM PBS, pH 8.0, 250 mM imidazole), the supernatants were subjected to 10% SDS-PAGE followed by Coomassie Brilliant Blue staining. The gel was excised, tryptic digest and subjected to LC-MS/MS analyzed by Shanghai Luming biological technology co., LTD (Shanghai, China) according to methods described elsewhere (Qin et al., 2019).

BiFC assay

Full-length cDNA of *FtSHMT* was amplified and inserted into the pSPYNE-35S vector. Full-length cDNA of *RsDAD* was amplified and inserted into the pSPYCE-35S vector. The constructs were introduced into *N. benthamiana* leaves using Agrobacterium (strain GV3101)-mediated infiltration. Fluorescence was observed using a laser scanning confocal microscope (Zeiss LSM900). Primer sequences are given in Supplemental Data Set S47.

Generation of transgenic lines and plant growth

Total RNA was extracted by using an RNApre Pure Plant Plus kit (DP441, Tiangen, Beijing, China); first-strand cDNA was synthesized with a HiScript III RT SuperMix for qPCR (R323-01, Vazyme, Nanjing, China). The coding sequence was cloned into pCAMBIA-1307. The *N. benthamiana* and Tartary buckwheat transient expression and the Arabidopsis (*Arabidopsis thaliana*) overexpression lines were conducted and generated by *Agrobacterium tumefaciens* (strain GV3101)-mediated transformation, respectively (Clough and Bent, 1998; Wang et al., 2023). Three biological replicates were conducted and the experiments were performed three times. Protein accumulation in *N. benthamiana* leaves was analyzed by immunoblotting with an anti-MBP (1:2000; CW0288M, CWBIO, Beijing, China) antibody. Relative expression levels of Arabidopsis heterologous expression lines were analyzed by RT-qPCR. Three biological replicates were conducted and the experiments were performed three times. Primer sequences are given in Supplemental Data Set S47. The T-DNA insertion mutants a*oc4* (SALK_124897C) and *jar1* (SALK_030821C) T-DNA were obtained from Arashare. The *myc2 myc3 myc4* triple mutant was described previously (Fernández-Calvo et al., 2011). All Arabidopsis genotypes were grown at 22℃ (day/night) under long-day conditions (16-h light/8-h dark). The phylogenetic tree of CYPs and ASPs were conducted using MEGA X based on the neighbor-joining method (Saitou and Nei 1987; Kumar et al. 2018). The unfiltered alignment and phylogenetic tree are provided as Supplemental Files 3 to 6.

Treatment with phytohormones

For Tartary buckwheat treated with different phytohormones, seven-day-old Tartary buckwheat seedlings were pre-treated with salicylic acid (1 mM, S7401, Sigma-Aldrich, Taufkirchen, Germany), MeJA (50 μM), gibberellin (100 μM, 48870, Sigma-Aldrich, Taufkirchen, Germany), ethephon (1 mM, C0143, Sigma-Aldrich, Taufkirchen, Germany) or DMSO (negative control) for 3 h. Phenotypes were observed

3 days after onset of *R. solani* AG4-HGI 3 infection. Three biological replicates were conducted and the experiments were performed three times.

For Arabidopsis mutants treated with JA, the detached leaves of two-week-old Arabidopsis seedlings were pre-treated with 50 μM MeJA or DMSO (negative control) for 3 h, and then inoculated with sub-cultured mycelial disks for 2 days. Wild-type (Col-0) seedlings were used as negative control. Three biological replicates were conducted and the experiments were performed three times.

Metabolome analysis of *FtCYP94C1* over-expressing Arabidopsis

Two-week-old Arabidopsis seedlings were used to conduct a widely targeted metabolite analysis (Want et al., 2010). Four independent biological replicates for each treatment were conducted. Each replicate was obtained by pooling samples from ten seedlings. Whole freeze-dried seedlings were ground and extracted with prechilled 80% (v/v) methanol/water. Following centrifugation at 15,000 g at 4℃ for 20 min, the supernatants were analyzed by using an ExionLC™ AD system (SCIEX) coupled with a QTRAP® 6500+ mass spectrometer (SCIEX) by Novogene Co., Ltd. (Beijing, China). The analytical conditions were as follows: column, Xselect HSS T3 (2.5 μm, 2.1×150 mm); solvent A, 0.1% (v/v) formic acid-water, and solvent B, 0.1% (v/v) formic acid-acetonitrile. The gradient program was as follows, 2% B, 2 min; 2-100% B, 15.0 min; 100% B, 17.0 min; 100-2% B, 17.1 min; 2% B, 20 min. The QTRAP® 6500+ mass spectrometer was operated in positive/negative polarity modes with curtain gas of 35 psi, collision gas of medium, ionspray voltage of 5500 V for positive and –4500V for negative, temperature of 550℃, ion source gas of 1: 60.

Qualitative analysis was performed using multiple reaction monitoring (MRM) based on the Novogene Database. The data files generated by HPLC-MS/MS were processed with SCIEX OS v1.4 to integrate and correct the peaks. The area of each peak represents the relative content of the corresponding metabolite. The metabolites were annotated using the KEGG database (http://www.genome.jp/kegg/), HMDB database (http://www.hmdb.ca/) and Lipidmaps database (https://www.lipidmaps.org/). Principal components analysis (PCA), partial least squares discriminant analysis (PLS-DA) and univariate analysis (*t*-test) were performed to identify the differentially abundant metabolites. The metabolites with VIP (variable importance for the projection) > 1, *P*-value < 0.05 and $|\log_2 FC| \geq 1$ were considered to be differentially abundant.

Flavonoids content analysis of Arabidopsis mutants

Flavonoid contents were analyzed according to the method described previously (Zhang et al., 2021; He et al., 2022). Two-week-old Arabidopsis seedlings were freeze-dried and ground. The powder was extracted with prechilled 80% (v/v) methanol/water. The supernatant was analyzed by LC-MS (Agilent G6500 Series HPLC-QTOF). The content of flavonoids was calculated by comparing the HPLC peak area with authentic standards (Sigma-Aldrich, Taufkirchen, Germany). Three biological replicates were conducted and each replicate was obtained by pooling samples from ten seedlings. The experiments were performed three times.

Screening candidate host plants and disease resistance evaluation

For *R. solani* and Tartary buckwheat interaction, Tartary buckwheat seeds were germinated in petri plates containing wet filter paper at 22℃. Seven days after germination, the seedlings were inoculated with 50 × diluted sub-cultured mycelial solution for 5 days. Three biological replicates using ten seedlings each were conducted. For validation of candidate virulence genes, detached transiently expressing *N. benthamiana* leaves were inoculated with sub-cultured mycelial disks for 2 days. Three biological replicates were conducted and the experiments were performed three times. For the *R. solani*–Arabidopsis interaction, detached leaves of two-week-old Arabidopsis seedlings were inoculated with sub-cultured mycelial disks for 2 days. Three biological replicates were conducted and the experiments were performed three times. For *R. solani* inoculation of other candidate host plant species, detached leaves of the appropriate size were inoculated with sub-cultured PDA mycelial disks. Plants inoculated with PDA or PDB medium without fungus were used as negative controls. Relative pathogen biomass was analyzed by measuring the abundance of the pathogen using qPCR of the internal transcribed spacer region (ITS) and normalized by plant biomass according the method described previously (Wallon et al., 2020). Three biological replicates were conducted and the experiments were performed three times. Primer sequences are listed in Supplemental Data Set S47. Disease index evaluation, 3,30-diaminobenzidine (DAB) staining and malondialdehyde (MDA) content analysis were conducted as previously described (Park et al., 2008; Bach-Pages et al., 2018; Yin et al., 2020). Three biological replicates were conducted and the experiments were performed three times.

Genome-wide association analysis

The resequencing data of 320 Tartary buckwheat accessions were obtained from published work (Zhang et al., 2021). GWAS was conducted using the method

previously illustrated in Zhang et al., 2021. Briefly, the sequenced reads of Tartary buckwheat accessions were mapped to the reference genome of Tartary buckwheat (HERA, Zhang et al., 2017) using BWA-MEM (Li et al., 2013). SNP calling was performed using the GATK pipeline (McKenna et al., 2010). After filtering (QUAL > 30.0, QD > 5.0, FS < 60.0, DP > 5), a total of 1,095,350 high-quality SNPs (MAF > 0.05 and missing rate < 0.01) for 320 accessions was used to perform GWAS. The algorithm Efficient Mixed-Model Association eXpedited (EMMAx) was used to conduct all associations (Kang et al., 2010), with a significance threshold set to $P = 1\times10^{-5}$.

Statistical analysis

Data of gene relative expression levels and disease index are shown as means ± standard deviation (SD). Significant differences were assessed using Chi-square tests, two-tailed Student's *t*-tests, one-way and two-way analysis of variance (ANOVA, $P = 0.01$) performed by SPSS22 software (SPSS, Chicago, IL, USA). Statistical data are provided as Supplemental Data Set 48.

Accession numbers

The genome sequencing data of this project are available from the National Center for Biotechnology Information under BioProject ID PRJNA917065. The raw transcriptome data of this project are available from the public database National Center for Biotechnology Information under BioProject ID PRJNA917064. The mass-spectrometry proteomics data are available from the ProteomeXchange Consortium via the PRIDE partner repository with the data set identifier PXD041641. The metabolome data are available from the CNCB under BioProject ID PRJCA016408.

Supplemental Data

Supplemental Figure S1. Phenotypes of crops inoculated with *R. solani* AG4-HGI 3.

Supplemental Figure S2. DAPI staining of nuclei in *R. solani* AG4-HGI 3 hyphae.

Supplemental Figure S3. K-mer analysis for estimating the genome size of *R. solani* AG4-HGI 3.

Supplemental Figure S4. Correlation between protein-coding gene number and genome size using linear regression analysis.

Supplemental Figure S5. Circos plot showing the distribution of genes (I), transposons (II), CAZymes (III), secreted proteins (IV), effectors (V), virulence genes (VI), the duplicated genes based on BUSCO (VII) and the syntenic relationship (inner Circos).

Supplemental Figure S6. Circos plot showing the syntenic relationship between genomes of different isolates of *R. solani*.

Supplemental Figure S7. The most significantly enriched GO terms in contracted gene families.

Supplemental Figure S8. Correlation between genome size and the number of pathogenicity genes using linear regression analysis.

Supplemental Figure S9. Phenotype of Tartary buckwheat seedlings inoculated with *R. solani* AG4-HGI 3.

Supplemental Figure S10. The most significantly enriched GO terms of upregulated genes in *R. solani* AG4-HGI 3 during infection of Tartary buckwheat.

Supplemental Figure S11. The most significantly enriched GO terms of expanded gene families with upregulated expression (up) or downregulated expression (down) in *R. solani* AG4-HGI 3 during infection of Tartary buckwheat.

Supplemental Figure S12. The most significantly enriched KEGG metabolic pathways of expanded gene families (up, upregulated expression; down, downregulated expression) in *R. solani* AG4-HGI 3 during infection of Tartary buckwheat.

Supplemental Figure S13. The most significantly enriched GO terms of contracted gene families with upregulated expression (up) or downregulated expression (down) in *R. solani* AG4-HGI 3 during infection of Tartary buckwheat.

Supplemental Figure S14. The most significantly enriched KEGG metabolic pathways of contracted gene families (up, upregulated expression; down, downregulated expression) in *R. solani* AG4-HGI 3 during infecting Tartary buckwheat.

Supplemental Figure S15. Immunoblot with anti-MBP antibody to detect virulence proteins following transient expression in *N. benthamiana* leaves.

Supplemental Figure S16. Phenotypes observed on *N. benthamiana* leaves transiently expressing virulence genes.

Supplemental Figure S17. Relative pathogen biomass of *R. solani* AG4-HGI 3 infecting *N. benthamiana* leaves transiently expressing virulence genes.

Supplemental Figure S18. MDA (malondialdehyde) content of *N. benthamiana* leaves transiently expressing virulence genes and infected with *R. solani* AG4-HGI 3.

Supplemental Figure S19. Subcellular localization of RsYTHDC and RsDAD.

Supplemental Figure S20. Immunoblot analysis with anti-His antibody to detect the purified recombinant His-RsYTHDC and His-RsDAD.

Supplemental Figure S21. BiFC assay showing interactions between FtSHMT and RsDAD in *N. benthamiana* leaf epidermal cells.

Supplemental Figure S22. The most significantly enriched GO terms of different expressed genes in Tartary buckwheat during infection by *R. solani* AG4-HGI 3.

Supplemental Figure S23. Phenotypes of Tartary buckwheat seedlings infected with *R. solani* AG4-HGI 3 and pre-treated with salicylic acid (SA), ethylene (ET), gibberellin (GA) or jasmonate acid (JA).

Supplemental Figure S24. The most significantly enriched GO terms of JA-induced differentially expressed genes in Tartary buckwheat during infection by *R. solani* AG4-HGI 3.

Supplemental Figure S25. RT-qPCR analysis of *FtCYP94C1* expression level in leaves of Arabidopsis lines heterologously expressing *FtCYP94C1*.

Supplemental Figure S26. Relative pathogen biomass of *R. solani* AG4-HGI 3 infected *FtCYP94C1* over-expression lines.

Supplemental Figure S27. DAB staining of Arabidopsis lines heterologously expressing *FtCYP94C1* and infected by *R. solani* AG4-HGI 3.

Supplemental Figure S28. Phenotypes observed on Tartary buckwheat leaves transiently overexpressing *FtCYP94C1* and infected by *R. solani* AG4-HGI 3.

Supplemental Figure S29. Phenotype of JA mutants (*aoc4*, *jar1* and *myc2 myc3 myc4*) and wild type (Col-0) plants inoculated with *R. solani* AG4-HGI 3 with or without pre-treatment with JA.

Supplemental Figure S30. Disease resistance of JA mutants (*aoc4*, *jar1* and *myc2 myc3 myc4*) and wild-type (Col-0) plants infected with *R. solani* AG4-HGI 3 with or without pre-treatment with JA.

Supplemental Figure S31. Relative pathogen biomass in JA mutants (*aoc4*, *jar1* and *myc2 myc3 myc4*) and wild-type (Col-0) plants inoculated with *R. solani* AG4-HGI 3 with or without pre-treatment with JA.

Supplemental Figure S32. Principal component analysis (PCA) for the metabolome data of Arabidopsis lines heterologously expressing *FtCYP94C1*. Wild-type (Col-0) plants were used as negative control.

Supplemental Figure S33. Flavonoids contents of JA mutants (*aoc4*, *jar1* and *myc2 myc3 myc4*) and wild type (Col-0) plants with or without pre-treatment with JA.

Supplemental Figure S34. Quantile-Quantile (Q-Q) plots of the disease index based on the EMMAx algorithm.

Supplemental Figure S35. The most significantly enriched KEGG metabolic pathways of GWAS-identified genes in Tartary buckwheat during *R. solani* infection.

Supplemental Figure S36. Overlapping GWAS signals between disease index and the content of disease resistance-associated metabolites (tangertin, indole and indole-3-carboxylic acid).

Supplemental Figure S37. RT-qPCR analysis of *FtASP* expression levels in leaves of Arabidopsis lines heterologously expressing *FtASP*.

Supplemental Figure S38. Phenotype of Arabidopsis lines heterologously expressing the indicated genes identified by GWAS upon infection with *R. solani* AG4-HGI 3.

Supplemental Figure S39. Disease resistance of Arabidopsis lines heterologously expressing the indicated genes identified by GWAS upon infection with *R. solani* AG4-HGI 3.

Supplemental Figure S40. Geographical distribution of Tartary buckwheat accessions.

Supplemental Figure S41. Relative pathogen biomass of Arabidopsis lines heterologously expressing *FtASP* and infected with *R. solani* AG4-HGI 3.

Supplemental Figure S42. DAB staining and MDA content of Arabidopsis lines heterologously expressing *FtASP1* infected with *R. solani* AG4-HGI 3.

Supplemental Figure S43. Phenotypes observed on Tartary buckwheat leaves transiently overexpressing *FtASP* infected with *R. solani* AG4-HGI 3.

Supplemental Figure S44. Immunoblotting with anti-His antibody to detect purified recombinant His-FtASP (1-225), His-FtASP-N (1-112) and His-FtASP-C (113-225).

Supplemental Figure S45. Biomass of *R. solani* AG4-HGI 3 grown for 24 h in PDB medium containing purified recombinant His-FtASP (1-225), His-FtASP-N (1-112) or His-FtASP-C (113-225).

Supplemental Figure S46. Protease activity assay of FtASP.

Supplemental Data Set S1. Summary of sequencing data of the *R. solani* AG4-HGI 3 assembly.

Supplemental Data Set S2. Genome survey data statistics with *k*-mer frequency distribution.

Supplemental Data Set S3. Description of the *R. solani* genome assembly.

Supplemental Data Set S4. Evaluation of *R. solani* AG4-HGI 3 sequencing results.

Supplemental Data Set S5. Summary of repeat elements in the *R. solani* AG4-HGI 3 assembly.

Supplemental Data Set S6. Summary of repeat elements in the genomes of 23 *R. solani* isolates and *M. oryzae*.

Supplemental Data Set S7. Orthologous gene families among 23 *R. solani* isolates and *M. oryzae*.

Supplemental Data Set S8. Number of gene families, specific family, genes in the family and unique genes of 23 *R. solani* isolates and *M. oryzae*.

Supplemental Data Set S9. List of expanded and contracted gene families in *R. solani* AG4-HGI 3.

Supplemental Data Set S10. Analysis of carbohydrate-active enzymes in *R. solani* AG4-HGI 3.

Supplemental Data Set S11. Characterization of carbohydrate-active enzymes in *R. solani*.

Supplemental Data Set S12. Characterization of carbohydrate-active enzymes involved in lignin, cellulose, hemicellulose and pectin degradation in *R. solani*.

Supplemental Data Set S13. Genes encoding predicted secreted proteins in *R. solani* AG4-HGI 3.

Supplemental Data Set S14. Predicted number of secreted proteins of *R. solani*.

Supplemental Data Set S15. Genes encoding predicted effector proteins in *R. solani* AG4-HGI 3.

Supplemental Data Set S16. Number of predicted effector proteins in *R. solani*.

Supplemental Data Set S17. Predicted virulence genes in *R. solani* AG4-HGI 3.

Supplemental Data Set S18. Genes encoding predicted interaction proteins between pathogens and plant hosts in *R. solani* AG4-HGI 3.

Supplemental Data Set S19. Genes encoding predicted transporters in *R. solani* AG4-HGI 3.

Supplemental Data Set S20. Genes encoding predicted transmembrane proteins in *R. solani* AG4-HGI 3.

Supplemental Data Set S21. Predicted secondary metabolite biosynthesis gene clusters in *R. solani* AG4-HGI 3.

Supplemental Data Set S22. Summary of RNA-seq results in *R. solani* AG4-HGI 3 after infection of Tartary buckwheat.

Supplemental Data Set S23. Upregulated genes in *R. solani* AG4-HGI 3 during the *R. solani*-Tartary buckwheat interaction.

Supplemental Data Set S24. Gene number with different expression pattern in expanded gene families.

Supplemental Data Set S25. Summary of expression pattern of expanded gene families.

Supplemental Data Set S26. Upregulated expanded gene families in *R. solani* AG4-HGI 3 during the *R. solani*-Tartary buckwheat interaction.

Supplemental Data Set S27. Downregulated expanded gene families in *R. solani* AG4-HGI 3 during the *R. solani*-Tartary buckwheat interaction.

Supplemental Data Set S28. Number of genes with different expression patterns in contracted gene families.

Supplemental Data Set S29. Summary of expression patterns of contracted gene families.

Supplemental Data Set S30. Upregulated contracted gene families in *R. solani* AG4-HGI 3 during the *R. solani*–Tartary buckwheat interaction.

Supplemental Data Set S31. Downregulated contracted gene families in *R. solani* AG4-HGI 3 during the *R. solani*–Tartary buckwheat interaction.

Supplemental Data Set S32. Upregulated genes encoding CAZymes in *R. solani* AG4-HGI 3 during *R. solani*–Tartary buckwheat interaction.

Supplemental Data Set S33. Number of upregulated genes encoding CAZymes in *R. solani* AG4-HGI 3 during infection of Tartary buckwheat.

Supplemental Data Set S34. Number of upregulated genes encoding CAZymes involved in lignin, cellulose, hemicellulose and pectin degradation in *R. solani* AG4-HGI 3 during infection of Tartary buckwheat.

Supplemental Data Set S35. Candidate interaction proteins of RsYTHDC in Tartary buckwheat identified by combination of pull down and mass spectrometry.

Supplemental Data Set S36. Candidate interaction proteins of RsDAD in Tartary buckwheat identified by combination of pull down and mass spectrometry.

Supplemental Data Set S37. Summary of RNA-seq results in Tartary buckwheat after infection by *R. solani* AG4-HGI 3.

Supplemental Data Set S38. Differentially expressed genes in Tartary buckwheat during the *R. solani*–Tartary buckwheat interaction.

Supplemental Data Set S39. Differentially expressed jasmonate acid biosynthesis and signaling genes in Tartary buckwheat during the *R. solani*–Tartary buckwheat interaction.

Supplemental Data Set S40. Summary of RNA-seq results in Tartary buckwheat after treatment with MeJA.

Supplemental Data Set S41. Differentially expressed Tartary buckwheat genes shared during the *R. solani*–Tartary buckwheat interaction and following MeJA treatment.

Supplemental Data Set S42. Metabolites with different abundance between *FtCYP4502* overexpression lines and WT.

Supplemental Data Set S43. Disease index of the 320 Tartary buckwheat accessions used in this study.

Supplemental Data Set S44. Candidate genes associated with disease resistance identified by GWAS.

Supplemental Data Set S45. Overlapping GWAS regions between disease resistance and disease resistance-associated metabolite content.

Supplemental Data Set S46. Candidate genes identified by GWAS with different expression levels during the *R. solani*–Tartary buckwheat interaction and following JA treatment.

Supplemental Data Set S47. Primers used in this study.

Supplemental Data Set S48. Summary of statistical analyses.

Supplemental File S1. Multiple sequence alignment for the phylogenetic tree shown in Figure 1A.

Supplemental File S2. Tree file for the phylogenetic tree shown in Figure 1A.

Supplemental File S3. Multiple sequence alignment for the phylogenetic tree shown in Figure 4A.

Supplemental File S4. Tree file for the phylogenetic tree shown in Figure 4A.

Supplemental File S5. Multiple sequence alignment for the phylogenetic tree shown in Figure 6C.

Supplemental File S6. Tree file for the phylogenetic tree shown in Figure 6C.

ACKNOWLEDGMENTS

This research was supported by National Natural Science Foundation of China (32161143005, 31901511, 31871536 and 31801427), the Project of Sanya Yazhou Bay Science and Technology City (SCKJ-JYRC-2022-22), the Youth Innovation Program of Chinese Academy of Agricultural Sciences (Y2022QC02), National Key R&D Program of China (2017YFE0117600, 2019YFD1000700/2019YFD1000701), European Union Horizon 2020 project Planta SYST (SGA-CSA No. 739582 under FPA

No.664620) and China National Postdoctoral Program for Innovative Talents (BX20200377).

AUTHORS CONTRIBUTIONS

M.Z. designed and managed the project. M.Z., A.R.F., M.A.C., and M.I.G. organized the funding for this research. J.C., B.X., and M.Z. provided the genetic materials. Y.H., K.Z., C.G., M.H., Y.S. and C.C performed data analysis and figure design. Y.H., S.L., X.L., H.Z., X.H., Z.K., Y.F., W.L., G.L., O.L and Y.C. performed most of the experiments. Y.H., K.Z., A.R.F., M.A.C., M.I.G., and M.Z. wrote the manuscript. All authors read and approved the manuscript.

REFERENCES

Anderson, J.P., Sperschneider, J., Win, J., Kidd, B., Yoshida, K., Hane, J., Saunders, D.G.O., and Singh, K.B. (2017). Comparative secretome analysis of *Rhizoctonia solani* isolates with different host ranges reveals unique secretomes and cell death inducing effectors. Sci. Rep. **7:** 10410.

Ao, Y., Li, Z., Feng, D., Xiong, F., Liu, J., Li, J.F., Wang, M., Wang, J., Liu, B., and Wang, H.B. (2014). OsCERK1 and OsRLCK176 play important roles in peptidoglycan and chitin signaling in rice innate immunity. Plant J. **80:** 1072-1084.

Armenteros, J.J.A., Tsirigos, K.D., Sønderby, C.K., Petersen, T.N., Winther, O., Brunak, S., von Heijne, G., and Nielsen, H. (2019). SignalP 5.0 improves signal peptide predictions using deep neural networks. Nat. Biotechnol. **37:** 420-423.

Bach-Pages, M., and Preston, G.M. (2018). Methods to quantify biotic-induced stress in plants. Methods Mol. Biol. **1734:** 241-255.

Bai, X., Zhan, G., Tian, S., Peng, H., Cui, X., Islam, M.A., Goher, F., Ma, Y., Kang, Z., Xu, Z.S., and Guo, J. (2021). Transcription factor BZR2 activates chitinase *Cht20.2* transcription to confer resistance to wheat stripe rust. Plant Physiol. **187:** 2749-2762.

Bari, R., and Jones, J.D. (2009). Role of plant hormones in plant defence responses. Plant Mol. Biol. **69:** 473-488.

Bienert, M.D., Siegmund, S.E., Drozak, A., Trombik, T., Bultreys, A., Baldwin, I.T., and Boutry, M. (2012). A pleiotropic drug resistance transporter in

Nicotiana tabacum is involved in defense against the herbivore *Manduca sexta*. Plant J. **72:** 745-757.

Borras-Hidalgo, O., Caprari, C., Hernandez-Estevez, I., Lorenzo, G.D., and Cervone, F. (2012). A gene for plant protection: expression of a bean polygalacturonase inhibitor in tobacco confers a strong resistance against *Rhizoctonia solani* and two oomycetes. Front. Plant Sci. **3:** 268.

Brymora, A., Valova, V.A., and Robinson, P.J. (2004). Protein-protein interactions identified by pull-down experiments and mass spectrometry. Curr. Protoc. Cell Biol. Capter 17, Unit 17.5.

Buchfink, B., Xie, C., and Huson, D.H. (2015). Fast and sensitive protein alignment using DIAMOND. Nat. Methods. **12:** 59-60.

Bundó, M., and Coca, M. (2016). Enhancing blast disease resistance by overexpression of the calcium-dependent protein kinase *OsCPK4* in rice. Plant Biotechnol. J. **14:** 1357-1367.

Bundó, M., and Coca, M. (2017). Calcium-dependent protein kinase OsCPK10 mediates both drought tolerance and blast disease resistance in rice plants. J. Exp. Bot. **68:** 2963-2975.

Cantarel, B.L., Coutinho, P.M., Rancurel, C., Bernard, T., Lombard, V., and Henrissat, B. (2009). The carbohydrate-active enzymes database (CAZy): an expert resource for glycogenomics. Nucleic Acids Res. **37:** D233-238.

Cantarel, B.L., Korf, I., Robb, S.M., Parra, G., Ross, E., Moore, B., Holt, C., Sánchez, A.A., and Yandell, M. (2008). MAKER: an easy-to-use annotation pipeline designed for emerging model organism genomes. Genome Res. **18:** 188-96.

Chen, C., Zhang, K., Khurshid, M., Li, J., and Zhou, M. (2019). MYB transcription repressors regulate plant secondary metabolism. Crit. Rev. Plant Sci. **38:** 159-170.

Chen, H., Li, C., Liu, L., Zhao, J., Cheng, X., Jiang, G., and Zhai, W. (2016). The Fd-GOGAT1 mutant gene *lc7* confers resistance to *Xanthomonas oryzae* pv. *Oryzae* in rice. Sci. Rep. **6:** 26411.

Chen, S., Zhou, Y., Chen, Y., and Gu, J. (2018). Fastp: an ultra-fast all-in-one FASTQ preprocessor. Bioinformatics. **34:** 884-890.

Choe, S., Choi, B., Kang, J.H., and Seo, J.K. (2021). Tolerance to tomato yellow leaf curl virus in transgenic tomato overexpressing a cellulose synthase-like gene. Plant

Biotechnol. J. **19:** 657-659.

Clough, S.J., and Bent, A.F. (1998). Floral dip: a simplified method for *Agrobacterium*-mediated transformation of *Arabidopsis thaliana*. Plant J. **16:** 735-743.

Cui, W., Wang, S., Han, K., Zheng, E., Ji, M., Chen, B., Wang, X., Chen, J., and Yan, F. (2021). Ferredoxin 1 is downregulated by the accumulation of abscisic acid in an ABI5-dependent manner to facilitate rice stripe virus infection in *Nicotiana benthamiana* and rice. Plant J. **107:** 1183-1197.

De Geyter, N., Gholami, A., Goormachtig, S., and Goossens, A. (2012). Transcriptional machineries in jasmonate-elicited plant secondary metabolism. Trends Plant Sci. **17:** 349-359.

Dean, R., Kan, J.A.V., Pretorius, Z.A., Hammond-Kosack, K.E., Pietro, A.D., Spanu, P.D., Rudd, J.J., Dickman, M., Kahmann, R., Ellis, J., and Foster, G.D. (2012). The Top 10 fungal pathogens in molecular plant pathology. Mol. Plant Pathol. **13:** 414-430.

Ding, M., Zhang, K., He, Y., Zuo, Q., Zhao, H., He, M., Georgiev, M.I., Park, S.U., and Zhou, M. (2021). FtBPM3 modulates the orchestration of FtMYB11-mediated flavonoids biosynthesis in Tartary buckwheat. Plant Biotechnol. J. **19:** 1285-1287.

Dong, C., Li, R., Wang, N., Liu, Y., Zhang, Y., and Bai, S. (2022). Apple vacuolar processing enzyme 4 modulates fruit disease resistance and is regulated by cysteine protease inhibitor. J. Exp. Bot. **73:** 3758-3773.

Dong, Z., Li, W., Liu, J., Li, L., Pan, S., Liu, S., Gao, J., Liu, L., Liu, X., Wang, G.L., and Dai, L. (2019). The rice phosphate transporter protein OsPT8 regulates disease resistance and plant growth. Sci. Rep. **9:** 5408.

Duan, H., et al. (2022). Physical separation of haplotypes in dikaryons allows benchmarking of phasing accuracy in Nanopore and HiFi assemblies with Hi-C data. Genome Biol. **23:** 84.

Eddy, S.R. (1998). Profile hidden Markov models. Bioinformatics. **14:** 755-763.

Edgar, R.C. (2004). MUSCLE: multiple sequence alignment with high accuracy and high throughput. Nucleic Acids Res. **32:** 1792-1797.

Feng, H., Wang, X., Zhang, Q., Fu, Y., Feng, C., Wang, B., Huang, L., and Kang, Z. (2014). Monodehydroascorbate reductase gene, regulated by the wheat PN-

2013 miRNA, contributes to adult wheat plant resistance to stripe rust through ROS metabolism. Biochim. Biophys. Acta. **1839:** 1-12.

Fernández-Calvo, P., et al. (2011). The Arabidopsis bHLH transcription factors MYC3 and MYC4 are targets of JAZ repressors and act additively with MYC2 in the activation of jasmonate responses. Plant Cell. **23:** 701-715.

Ferrari, S., Vairo, D., Ausubel, F.M., Cervone, F., and De Lorenzo, G. (2003). Tandemly duplicated Arabidopsis genes that encode polygalacturonase-inhibiting proteins are regulated coordinately by different signal transduction pathways in response to fungal infection. Plant Cell **15:** 93-106.

Gamir, J., Pastor, V., Cerezo, M., and Flors, V. (2012). Identification of indole-3-carboxylic acid as mediator of priming against *Plectosphaerella cucumerina*. Plant Physiol. Biochem. **61:** 169-179.

Ger, M.J., Louh, G.Y., Lin, Y.H., Feng, T.Y., and Huang, H.E. (2014). Ectopically expressed sweet pepper ferredoxin PFLP enhances disease resistance to *Pectobacterium carotovorum* subsp. *carotovorum* affected by harpin and protease-mediated hypersensitive response in Arabidopsis. Mol. Plant Pathol. **15:** 892-906.

Hane, J.K., Anderson, J.P., Williams, A.H., Sperschneider, J., and Singh, K.B. (2014). Genome sequencing and comparative genomics of the broad host-range pathogen *Rhizoctonia solani* AG8. PLoS Genet. **10:** e1004281.

He M, He Y, Zhang K, Lu X, Zhang X, Gao B, Fan Y, Zhao H, Jha R, Huda MN, Tang Y, Wang J, Yang W, Yan M, Cheng J, Ruan J, Dulloo E, Zhang Z, Georgiev MI, Chapman MA, Zhou M. Comparison of buckwheat genomes reveals the genetic basis of metabolomic divergence and ecotype differentiation. New Phytol. 2022:235(5):1927-1943. https://doi.org/10.1111/nph.18306

He, Y., Wu, L., Liu, X., Jiang, P., Yu, L., Qiu, J., Wang, G., Zhang, X., and Ma, H. (2020). *TaUGT6*, a novel UDP-glycosyltransferase gene enhances the resistance to FHB and DON accumulation in wheat. Front. Plant Sci. **11:** 574775.

Heitz, T., Widemann, E., Lugan, R., Miesch, L., Ullmann, P., Désaubry, L., Holder, E., Grausem, B., Kandel, S., Miesch, M., Werck-Reichhart, D., and Pinot, F. (2012). Cytochromes P450 CYP94C1 and CYP94B3 catalyze two successive oxidation steps of plant hormone jasmonoyl-isoleucine for catabolic turnover. J. Biol. Chem. **287:** 6296-6306.

Hernández-Blanco, C., et al. (2007). Impairment of cellulose synthases required for *Arabidopsis* secondary cell wall formation enhances disease resistance. Plant Cell **19:** 890-903.

Hu, P., Meng, Y., and Wise, R.P. (2009). Functional contribution of chorismate synthase, anthranilate synthase, and chorismate mutase to penetration resistance in barley-powdery mildew interactions. Mol. Plant Microbe. Interact. **22:** 311-320.

Huang, H.E., Ger, M.J., Chen, C.Y., Pandey, A.K., Yip, M.K., Chou, H.W., and Feng, T.Y. (2007). Disease resistance to bacterial pathogens affected by the amount of ferredoxin-I protein in plants. Mol. Plant Pathol. **8:** 129-137.

Jones, P., et al. (2014). InterProScan 5: genome-scale protein function classification. Bioinformatics. **30:** 1236-1240.

Kang, H.M., Sul, J.H., Service, S.K., Zaitlen, N.A., Kong, S.Y., Freimer, N.B., Sabatti, C., and Eskin, E. (2010). Variance component model to account for sample structure in genome-wide association studies. Nat. Genet. **42:** 348-354.

Kankanala, P., Nandety, R.S., and Mysore, K.S. (2019). Genomics of plant disease resistance in legumes. Front. Plant Sci. **10:** 1345.

Karki, S.J., Reilly, A., Zhou, B., Mascarello, M., Burke, J., Doohan, F., Douchkov, D., Schweizer, P., and Feechan, A. (2021). A small secreted protein from *Zymoseptoria tritici* interacts with a wheat E3 ubiquitin ligase to promote disease. J. Exp. Bot. **72:** 733-746.

Kaushik, A., Roberts, D.P., Ramaprasad, A., Mfarrej, S., Nair, M., Lakshman, D.K, and Pain, A. (2022). Pangenome analysis of the soilborne fungal phytopathogen *Rhizoctonia solani* and development of a comprehensive web resource: RsolaniDB. Front. Microbiol. **13:** 839524.

Khare, D., Choi, H., Huh, S.U., Bassin, B., Kim, J., Martinoia, E., Sohn, K.H., Paek, K.H., and Lee, Y. (2017). *Arabidopsis* ABCG34 contributes to defense against necrotrophic pathogens by mediating the secretion of camalexin. Proc. Natl. Acad. Sci. USA **114:** 5712-5720.

Kim, D., Langmead, B., and Salzberg, S.L. (2015). HISAT: a fast spliced aligner with low memory requirements. Nat. Methods. **12:** 357-360.

Ko, M., Cho, J.H., Seo, H.H., Lee, H.H., Kang, H.Y., Nguyen, T.S., Soh, H.C., Kim,

Y.S., and Kim, J.I. (2016). Constitutive expression of a fungus-inducible carboxylesterase improves disease resistance in transgenic pepper plants. Planta. **244:** 379-392.

Koo, A.J., Cooke, T.F., and Howe, G.A. (2011). Cytochrome P450 CYP94B3 mediates catabolism and inactivation of the plant hormone jasmonoyl-L-isoleucine. Proc. Natl. Acad. Sci. USA **108:** 9298-9303.

Koo, A.J, Thireault, C., Zemelis, S., Poudel, A.N., Zhang, T., Kitaoka, N., Brandizzi, F., Matsuura, H., and Howe, G.A. (2014). Endoplasmic reticulum-associated inactivation of the hormone jasmonoyl-L-isoleucine by multiple members of the cytochrome P450 94 family in *Arabidopsis*. J. Biol. Chem. **289:** 29728-29738.

Koren, S., Walenz, B.P., Berlin, K., Miller, J.R., Bergman, N.H., and Phillippy, A.M. (2017). Canu: scalable and accurate long-read assembly via adaptive *k*-mer weighting and repeat separation. Genome Res. **27:** 722-736.

Kouzai, Y., et al. (2018). Salicylic acid-dependent immunity contributes to resistance against *Rhizoctonia solani*, a necrotrophic fungal agent of sheath blight, in rice and *Brachypodium distachyon*. New Phytol. **217:** 771-783.

Kumar, S., Stecher, G., Li, M., Knyaz, C., and Tamura, K. (2018). MEGA X: Molecular evolutionary genetics analysis across computing platforms. Mol. Biol. Evol. **35:** 1547-1549.

Kurtz, S., Phillippy, A., Delcher, A.L., Smoot, M., Shumway, M., Antonescu, C., and Salzberg, S.L. (2004). Versatile and open software for comparing large genomes. Genome Biol. **5:** R12.

Lee, D.Y., et al. (2021). Comparative genome analyses of four rice-infecting *Rhizoctonia solani* isolates reveal extensive enrichment of homogalacturonan modification genes. BMC Genomics. **22:** 242.

Li, B., and Dewey, C.N. (2011). RSEM: accurate transcript quantification from RNA-Seq data with or without a reference genome. BMC Bioinformatics. **12:** 323.

Li, C., Guo, Z., Zhou, S., Han, Q., Zhang, M., Peng, Y., Hsiang, T., and Chen, X. (2021). Evolutionary and genomic comparisons of hybrid uninucleate and nonhybrid *Rhizoctonia* fungi. Commun Biol. **4:** 201.

Li, D., Li, S., Wei, S., and Sun, W. (2021). Strategies to manage rice sheath blight: Lessons from interactions between rice and *Rhizoctonia solani*. Rice. **14:** 21.

Li, H. (2013). Aligning sequence reads, clone sequences and assembly contigs with

BWA-MEM. arXiv:1303.3997v2.

Li, L., Stoeckert, C.J.J, and Roos, D.S. (2003). OrthoMCL: identification of ortholog groups for eukaryotic genomes. Genome Res. **13:** 2178-2189.

Li, N., Lin, B., Wang, H., Li, X., Yang, F., Ding, X., Yan, J., and Chu, Z. (2019). Natural variation in *ZmFBL41* confers banded leaf and sheath blight resistance in maize. Nat. Genet. **51:** 1540-1548.

Li, R., et al. (2010). De novo assembly of human genomes with massively parallel short read sequencing. Genome Res. **20:** 265-272.

Li, S., Zhang, K., Khurshid, M., Fan, Y., Xu, B., and Zhou, M. (2020). First report of *Rhizoctonia solani* AG-4 HGI causing stem canker on *Fagopyrum tataricum* (Tartary buckwheat) in China. Plant Dis. https://doi.org/10.1094/PDIS-06-20-1253-PDN.

Liang, M., Ye, H., Shen, Q., Jiang, X., Cui, G., Gu, W., Zhang, L.H., Naqvi, N.I., and Deng, Y.Z. (2021). Tangeretin inhibits fungal ferroptosis to suppress rice blast. J. Integr. Plant Biol. **63:** 2136-2149.

Liu, F., Huang, N., Wang, L., Ling, H., Sun, T., Ahmad, W., Muhammad, K., Guo, J., Xu, L., Gao, S., Que, Y., and Su, Y. (2018). A novel L-ascorbate peroxidase 6 gene, *ScAPX6*, plays an important role in the regulation of response to biotic and abiotic stresses in sugarcane. Front. Plant Sci. **8:** 2262.

Liu, H., Ma, Y., Chen, N., Guo, S., Liu, H., Guo, X., Chong, K., and Xu, Y. (2014). Overexpression of stress-inducible OsBURP16, the β subunit of polygalacturonase 1, decreases pectin content and cell adhesion and increases abiotic stress sensitivity in rice. Plant Cell Environ. **37:** 1144-1158.

Liu, S., et al. (2021). A single-nucleotide mutation in a GLUTAMATE RECEPTOR-LIKE gene confers resistance to Fusarium Wilt in *Gossypium hirsutum*. Adv. Sci. **8:** 2002723.

Love, M.I., Huber, W., and Anders, S. (2014). Moderated estimation of fold change and dispersion for RNA-seq data with DESeq2. Genome Biol. **15:** 550.

Lowe, T.M., and Eddy, S.R. (1997). TRNAscan-SE: a program for improved detection of transfer RNA genes in genomic sequence. Nucleic Acids Res. **25:** 955-964.

Lu, Y.J., Li, P., Shimono, M., Corrion, A., Higaki, T., He, S.Y., and Day, B. (2020). Arabidopsis calcium-dependent protein kinase 3 regulates actin cytoskeleton organization and immunity. Nat. Commun. **11:** 6234.

Mat Razali, N., Hisham, S.N., Kumar, I.S., Shukla, R.N., Lee, M., Abu Bakar, M.F., and Nadarajah, K. (2021). Comparative genomics: Insights on the pathogenicity and lifestyle of *Rhizoctonia solani*. Int. J. Mol. Sci. **22:** 2183.

McKenna, A., Hanna, M., Banks, E., Sivachenko, A., Cibulskis, K., Kernytsky, A., Garimella, K., Altshuler, D., Gabriel, S., Daly, M., and DePristo, M.A. (2010). The genome analysis toolkit: a MapReduce framework for analyzing next-generation DNA sequencing data. Genome Res. **20:** 1297-1303.

Mhamdi, A., Mauve, C., Gouia, H., Saindrenan, P., Hodges, M., and Noctor, G. (2010). Cytosolic NADP-dependent isocitrate dehydrogenase contributes to redox homeostasis and the regulation of pathogen responses in *Arabidopsis* leaves. Plant Cell Environ. **33:** 1112-1123.

Misra, P., Pandey, A., Tiwari, M., Chandrashekar, K., Sidhu, O.P., Asif, M.H., Chakrabarty, D., Singh, P.K., Trivedi, P.K., Nath, P., and Tuli, R. (2010). Modulation of transcriptome and metabolome of tobacco by Arabidopsis transcription factor, *AtMYB12*, leads to insect resistance. Plant Physiol. **152:** 2258-2268.

Moeder, W., Urquhart, W., Ung, H., and Yoshioka, K. (2011). The role of cyclic nucleotide-gated ion channels in plant immunity. Mol. Plant **4:** 442-452.

Molla, K.A, Karmakar, S., Molla, J., Bajaj, P., Varshney, R.K., Datta, S.K., and Datta, K. (2020). Understanding sheath blight resistance in rice: the road behind and the road ahead. Plant Biotechnol. J. **18:** 895-915.

Moreno, J.I., Martín, R., and Castresana, C. (2005). Arabidopsis SHMT1, a serine hydroxymethyltransferase that functions in the photorespiratory pathway influences resistance to biotic and abiotic stress. Plant J. **41:** 451-463.

Mutuku, J.M., and Nose, A. (2012). Changes in the contents of metabolites and enzyme activities in rice plants responding to *Rhizoctonia solani* Kuhn infection: activation of glycolysis and connection to phenylpropanoid pathway. Plant Cell Physiol. **53:** 1017-1032.

Myers, E.W. et al. (2000). A whole-genome assembly of *Drosophila*. Science. 287: 2196-2204.

Oh, S.K., Baek, K.H., Seong, E.S., Joung, Y.H., Choi, G.J., Park, J.M., Cho, H.S., Kim, E.A., Lee, S., and Choi, D. (2010). CaMsrB2, pepper methionine sulfoxide reductase B2, is a novel defense regulator against oxidative stress and pathogen attack. Plant Physiol. **154:** 245-261.

Pan, L., Zhao, X., Chen, M., Fu, Y., Xiang, M., and Chen, J. (2020). Effect of exogenous methyl jasmonate treatment on disease resistance of postharvest kiwifruit. Food Chem. **305:** 125483.

Pandey, S.P., and Somssich, I.E. (2009). The role of WRKY transcription factors in plant immunity. **Plant Physiol. 150:** 1648-1655.

Paparella, C., Savatin, D.V., Marti, L., De Lorenzo, G., and Ferrari, S. (2014). The Arabidopsis LYSIN MOTIF-CONTAINING RECEPTOR-LIKE KINASE3 regulates the cross talk between immunity and abscisic acid responses. Plant Physiol. **165:** 262-276.

Park, D.S., Sayler, R.J., Hong, Y.G., Nam, M.H., and Yang, Y. (2008). A method for inoculation and evaluation of rice sheath blight disease. Plant Dis. **92:** 25-29.

Pasquet, J.C., Changenet, V., Macadré, C., Boex-Fontvieille, E., Soulhat, C., Bouchabké-Coussa, O., Dalmais, M., Atanasova-Pénichon, V., Bendahmane, A., Saindrenan, P., and Dufresne, M. (2016). A *Brachypodium* UDP-glycosyltransferase confers root tolerance to deoxynivalenol and resistance to *Fusarium* infection. Plant Physiol. **172:** 559-574.

Pastor-Fernández, J., Pastor, V., Mateu, D., Gamir, J., Sánchez-Bel, P., and Flors, V. (2019). Accumulating evidences of callose priming by indole- 3-carboxylic acid in response to *Plectospharella cucumerina*. Plant Signal. Behav. **14:** 1608107.

Peng, C., Liang, X., Liu, E.E., Zhang, J.J., and Peng, X.X. (2017). The oxalyl-CoA synthetase-regulated oxalate and its distinct effects on resistance to bacterial blight and aluminium toxicity in rice. Plant Biol. (Stuttg). **19:** 345-353.

Pertea, M., Pertea, G.M., Antonescu, C.M., Chang, T.C., Mendell, J.T., and Salzberg, S.L. (2015). StringTie enables improved reconstruction of a transcriptome from RNA-seq reads. Nat. Biotechnol. **33:** 290-295.

Poudel, A.N., Holtsclaw, R.E., Kimberlin, A., Sen, S., Zeng, S., Joshi, T., Lei, Z., Sumner, L.W., Singh, K., Matsuura, H., and Koo, A.J. (2019). 12-hydroxy-jasmonoyl-l-isoleucine is an active jasmonate that signals through CORONATINE

INSENSITIVE 1 and contributes to the wound response in Arabidopsis. Plant Cell Physiol. **60:** 2152-2166.

Prasad, B.D., Creissen, G., Lamb, C., and Chattoo, B.B. (2009). Overexpression of rice (*Oryza sativa* L.) *OsCDR1* leads to constitutive activation of defense responses in rice and *Arabidopsis*. Mol. Plant Microbe. Interact. **22:** 1635-1644.

Qin, X., Pi, X., Wang, W., Han, G., Zhu, L., Liu, M., Cheng, L., Shen, J., Kuang, T., and Sui, S. (2019). Structure of a green algal photosystem I in complex with a large number of light-harvesting complex I subunits. Nat. Plants. **5:** 263-272.

Rhie, A., Walenz, B.P., Koren, S., and Phillippy, A.M. (2020). Merqury: reference-free quality, completeness, and phasing assessment for genome assemblies. Genome Biol. **21:** 245.

Robinson, M.D., McCarthy, D.J., and Smyth, G.K. (2010). edgeR: a Bioconductor package for differential expression analysis of digital gene expression data. Bioinformatics. **26:** 139-140.

Saitou, N., and Nei, M. (1987). The neighbor-joining method: a new method for reconstructing phylogenetic trees. Mol Biol Evol. **4:** 406-425.

Sasse, J., Schlegel, M., Borghi, L., Ullrich, F., Lee, M., Liu, G.W., Giner, J.L., Kayser, O., Bigler, L., Martinoia, E., and Kretzschmar, T. (2016). *Petunia hybrida* PDR2 is involved in herbivore defense by controlling steroidal contents in trichomes. Plant Cell Environ. **39:** 2725-2739.

Schenke, D., Utami, H.P., Zhou, Z., Gallegos, M.T., and Cai, D. (2019). Suppression of UV-B stress induced flavonoids by biotic stress: Is there reciprocal crosstalk? Plant Physiol. Biochem. **134:** 53-63.

Seemann, T. (2014). Prokka: rapid prokaryotic genome annotation. Bioinformatics. **30:** 2068-2069.

Shen, Q., Liu, L., Wang, L., and Wang, Q. (2018). Indole primes plant defense against necrotrophic fungal pathogen infection. PLoS One. 13: e0207607.

Shi, H., Liu, W., Yao, Y., Wei, Y., and Chan, Z. (2017). *Alcohol dehydrogenase 1* (*ADH1*) confers both abiotic and biotic stress resistance in *Arabidopsis*. Plant Sci. **262:** 24-31.

Shu, X., et al. (2021). Genome-wide association study and transcriptome analysis discover new genes for bacterial leaf blight resistance in rice (*Oryza sativa* L.). BMC Plant Biol. **21:** 255.

Sperschneider, J., and Dodds, P.N. (2022). EffectorP 3.0: Prediction of apoplastic and cytoplasmic effectors in fungi and oomycetes. Mol. Plant Microbe Interact. **35:** 146-156.

Stamatakis, A. (2014). RAxML version 8: a tool for phylogenetic analysis and post-analysis of large phylogenies. Bioinformatics. 30: 1312-1213.

Taheri, P., and Tarighi, S. (2010). Riboflavin induces resistance in rice against *Rhizoctonia solani via* jasmonate-mediated priming of phenylpropanoid pathway. J. Plant Physiol. **167:** 201-208.

Takashima, M., Sriswasdi, S., Manabe, R.I., Ohkuma, M., Sugita, T. and Iwasaki, W. (2018). A Trichosporonales genome tree based on 27 haploid and three evolutionarily conserved 'natural' hybrid genomes. Yeast. **35:** 99-111.

Tarailo-Graovac, M., and Chen, N. (2009). Using RepeatMasker to identify repetitive elements in genomic sequences. Curr. Protoc. Bioinformatics. Chapter 4: 4.10.1-4.10.14.

Tian, S., Wang, X., Li, P., Wang, H., Ji, H., Xie, J., Qiu, Q., Shen, D., and Dong, H. (2016). Plant aquaporin AtPIP1;4 links apoplastic H_2O_2 induction to disease immunity pathways. Plant Physiol. **171:** 1635-1650.

Ullah, C., Unsicker, S.B., Fellenberg, C., Constabel, C.P., Schmidt, A., Gershenzon, J., and Hammerbacher, A. (2017). Flavan-3-ols are an effective chemical defense against rust infection. Plant Physiol. **175:** 1560-1578.

Vaser, R., Sović, I., Nagarajan, N., and Šikić, M. (2017). Fast and accurate de novo genome assembly from long uncorrected reads. Genome Res. **27:** 737-746.

Verma, V., Ravindran, P., and Kumar, P.P. (2016). Plant hormone-mediated regulation of stress responses. BMC Plant Biol. **16:** 86.

Vurture GW, Sedlazeck FJ, Nattestad M, Underwood CJ, Fang H, Gurtowski J, Schatz MC. GenomeScope: fast reference-free genome profiling from short reads. Bioinformatics. 2017:33(14):2202-2204.

Waghu, F.H. and Idicula-Thomas, S. (2020). Collection of antimicrobial peptides database and its derivatives: Applications and beyond. Protein Sci. **29:** 36-42.

Wallon, T., Sauvageau, A., and Heyden, H.V. (2020). Detection and quantification of *Rhizoctonia solani* and *Rhizoctonia solani* AG1-IB causing the bottom rot of lettuce in tissues and soils by multiplex qPCR. Plants (Basel). **10:** 57.

Wally, O., and Punja, Z.K. (2010). Enhanced disease resistance in transgenic carrot (*Daucus carota* L.) plants over-expressing a rice cationic peroxidase. Planta. **232:** 1229-1239.

Wan, J., Tanaka, K., Zhang, X.C., Son, G.H., Brechenmacher, L., Nguyen, T.H., and Stacey, G. (2012). LYK4, a lysin motif receptor-like kinase, is important for chitin signaling and plant innate immunity in Arabidopsis. Plant Physiol. **160:** 396-406.

Wang, A., et al. (2021a). Identification of rice (*Oryza sativa* L.) genes involved in sheath blight resistance via a genome-wide association study. Plant Biotechnol. J. **19:** 1553-1566.

Wang, L., Feng, Z., Wang, X, and Zhang X. (2010). DEGseq: an R package for identifying differentially expressed genes from RNA-seq data. Bioinformatics, 26: 136-138.

Wang, J., et al. (2019a). A cyclic nucleotide-gated channel mediates cytoplasmic calcium elevation and disease resistance in rice. Cell Res. **29:** 820-831.

Wang, K., Shao, Z., Guo, F., Wang, K., and Zhang, Z. (2021b). The mitogen-activated protein kinase kinase TaMKK5 mediates immunity via the TaMKK5-TaMPK3-TaERF3 module. Plant Physiol. **187:** 2323-2337.

Wang, M., Rui, L., Yan, H., Shi, H., Zhao, W., Lin, J.E., Zhang, K., Blakeslee, J.J., Mackey, D., Tang, D., Wei, Z., and Wang, G.L. (2018). The major leaf ferredoxin Fd2 regulates plant innate immunity in Arabidopsis. Mol. Plant Pathol. **19:** 1377-1390.

Wang, W., Cai, J., Wang, P., Tian, S., and Qin, G. (2017). Post-transcriptional regulation of fruit ripening and disease resistance in tomato by the vacuolar protease SlVPE3. Genome Biol. **18:** 47.

Wang, X., Prokhnevsky, A.I., Skarjinskaia, M., Razzak, M.A., Streatfield, S.J., and Lee, J.Y. (2023). Facilitating viral vector movement enhances heterologous protein production in an established plant system. Plant Biotechnol. J. **21:** 635-645.

Wang, X., Zhi, P., Fan, Q., Zhang, M., and Chang, C. (2019b). Wheat CHD3 protein TaCHR729 regulates the cuticular wax biosynthesis required for stimulating germination of *Blumeria graminis* f.sp. *tritici*. J. Exp. Bot. **70:** 701-713.

Wang, Z., et al. (2022). An aspartic protease 47 causes quantitative recessive resistance to rice black-streaked dwarf virus disease and southern rice black-streaked dwarf virus disease. New Phytol. **233:** 2520-2533.

Wangdi, T., Uppalapati, S.R., Nagaraj, S., Ryu, C.M., Bender, C.L., and Mysore, K.S. (2010). A virus-induced gene silencing screen identifies a role for *Thylakoid Formation1* in *Pseudomonas syringae* pv *tomato* symptom development in tomato and Arabidopsis. Plant Physiol. **152:** 281-292.

Want, E.J., Wilson, I.D., Gika, H., Theodoridis, G., Plumb, R.S., Shockcor, J., Holmes, E., and Nicholson, J.K. (2010). Global metabolic profiling procedures for urine using UPLC-MS. Nat. Protoc. **5:** 1005-1018.

Wei, X., Shen, F., Hong, Y., Rong, W., Du, L., Liu, X., Xu, H., Ma, L., and Zhang, Z. (2016). The wheat calcium-dependent protein kinase TaCPK7-D positively regulates host resistance to sharp eyespot disease. Mol. Plant Pathol. **17:** 1252-1264.

Weidenbach, D., et al. (2014). Evolutionary conserved function of barley and Arabidopsis 3-KETOACYL-CoA SYNTHASES in providing wax signals for germination of powdery mildew fungi. Plant Physiol. **166:** 1621-1633.

Wen, Z., et al. (2018). Integrating GWAS and gene expression data for functional characterization of resistance to white mould in soya bean. Plant Biotechnol. J. **16:** 1825-1835.

Wibberg, D., Andersson, L., Tzelepis, G., Rupp, O., Blom, J., Jelonek, L., Pühler, A., Fogelqvist, J., Varrelmann, M., Schlüter, A., and Dixelius, C. (2016). Genome analysis of the sugar beet pathogen *Rhizoctonia solani* AG2-2IIIB revealed high numbers in secreted proteins and cell wall degrading enzymes. BMC Genomics. **17:** 245.

Wibberg, D., Genzel, F., Verwaaijen, B., Blom, J., Rupp, O., Goesmann, A., Zrenner, R., Grosch, R., Pühler, A., and Schlüter, A. (2017). Draft genome sequence of the potato pathogen *Rhizoctonia solani* AG3-PT isolate Ben3. Arch. Microbiol. **199:** 1065-1068.

Wibberg, D., Jelonek, L., Rupp, O., Hennig, M., Eikmeyer, F., Goesmann, A., Hartmann, A., Borriss, R., Grosch, R., Pühler, A., and Schlüter, A. (2013). Establishment and interpretation of the genome sequence of the phytopathogenic fungus *Rhizoctonia solani* AG1-IB isolate 7/3/14. J. Biotechnol. **167:** 142-155.

Wibberg, D., Rupp, O., Jelonek, L., Kröber, M., Verwaaijen, B., Blom, J., Winkler, A., Goesmann, A., Grosch, R., Pühler, A., and Schlüter, A. (2015). Improved genome sequence of the phytopathogenic fungus *Rhizoctonia solani* AG1-IB 7/3/14 as established by deep mate-pair sequencing on the MiSeq (Illumina) system. J. Biotechnol. **203:** 19-21.

Winnenburg, R., Baldwin, T.K., Urban, M., Rawlings, C., Köhler, J., and Hammond-Kosack, K.E. (2006). PHI-base: a new database for pathogen host interactions. Nucleic Acids Res. **34:** 459-464.

Wu, Y., Zhang, L., Zhou, J., Zhang, X., Feng, Z., Wei, F., Zhao, L., Zhang, Y., Feng, H., and Zhu, H. (2021). Calcium-dependent protein kinase GhCDPK28 was dentified and involved in Verticillium Wilt resistance in cotton. Front. Plant Sci. **12:** 772649.

Xia, Y., Fei, B., He, J., Zhou, M., Zhang, D., Pan, L., Li, S., Liang, Y., Wang, L., Zhu, J., Li, P., and Zheng, A. (2017). Transcriptome analysis reveals the host selection fitness mechanisms of the *Rhizoctonia solani* AG1IA pathogen. Sci. Rep. **7:** 10120.

Xia, Y., Suzuki, H., Borevitz, J., Blount, J., Guo, Z., Patel, K., Dixon, R.A., and Lamb, C. (2004). An extracellular aspartic protease functions in *Arabidopsis* disease resistance signaling. EMBO J. **23:** 980-988.

Yamamoto, M., Nakatsuka, S., Otani, H., Kohmoto, K., and Nishimura, S. (2000). (+)-catechin acts as an infection-inhibiting factor in strawberry leaf. Phytopathology. **90:** 595-600.

Yang, C.L., Liang, S., Wang, H.Y., Han, L.B., Wang, F.X., Cheng, H.Q., Wu, X.M., Qu, Z.L., Wu, J.H., and Xia, G.X. (2015). Cotton major latex protein 28 functions as a positive regulator of the ethylene responsive factor 6 in defense against *Verticillium dahliae*. Mol. Plant. **8:** 399-411.

Yang, G., and Li, C. (2012). General description of *Rhizoctonia* species complex. In: Plant pathology: INTECH Open Access Publisher.

Yang, W., Xu, X., Li, Y., Wang, Y., Li, M., Wang, Y., Ding, X., and Chu, Z. (2016). Rutin-mediated priming of plant resistance to three bacterial pathogens initiating the early SA signal pathway. PLoS One. **11:** e0146910.

Yao, L., Li, Y., Ma, C., Tong, L., Du, F., and Xu, M. (2020). Combined genome-wide association study and transcriptome analysis reveal candidate genes for resistance

to *Fusarium* ear rot in maize. J. Integr. Plant. Biol. **62:** 1535-1551.

Ye, J., Ding, W., Chen, Y., Zhu, X., Sun, J., Zheng, W., Zhang, B., and Zhu, S. (2020). A nucleoside diphosphate kinase gene *OsNDPK4* is involved in root development and defense responses in rice (*Oryza sativa* L.). Planta. **251:** 77.

Yin, W., et al. (2020). ARGONAUTE2 enhances grain length and salt tolerance by activating *BIG GRAIN3* to modulate cytokinin distribution in rice. Plant Cell. **32:** 2292-2306.

Yu, H.S., Ma, L.Q., Zhang, J.X., Shi, G.L., Hu, Y.H., and Wang, Y.N. (2011). Characterization of glycosyltransferases responsible for salidroside biosynthesis in *Rhodiola sachalinensis*. Phytochemistry **72:** 862-70.

Yu, Y., Ouyang, Y., and Yao, W. (2018). shinyCircos: an R/Shiny application for interactive creation of Circos plot. Bioinformatics. 34: 1229-1231.

Zhang, C., Gao, H., Li, R., Han, D., Wang, L., Wu, J., Xu, P., and Zhang, S. (2019a). GmBTB/POZ, a novel BTB/POZ domain-containing nuclear protein, positively regulates the response of soybean to *Phytophthora sojae* infection. Mol. Plant Pathol. **20:** 78-91.

Zhang, H., Yohe, T., Huang, L., Entwistle, S., Wu, P., Yang, Z., Busk, P.K., Xu, Y., and Yin, Y. (2018). dbCAN2: a meta server for automated carbohydrate-active enzyme annotation. Nucleic Acids Res. **46:** 95-101.

Zhang, Y.L., Zhang, C.L., Wang, G.L., Wang, Y.X., Qi, C.H., Zhao, Q., You, C.X., Li, Y.Y., and Hao, Y.J. (2019b). The R2R3 MYB transcription factor MdMYB30 modulates plant resistance against pathogens by regulating cuticular wax biosynthesis. BMC Plant Biol. **19:** 362.

Zhang, K., et al. (2021). Resequencing of global Tartary buckwheat accessions reveals multiple domestication events and key loci associated with agronomic traits. Genome Biol. **22:** 23.

Zhang, K., Logacheva, M.D., Meng, Y., Hu, J., Wan, D., Li, L., Dagmar, J., Wang, Z., Georgiev, M.I., and Yu, Z. (2018). Jasmonate-responsive MYB factors spatially repress rutin biosynthesis in *Fagopyrum tataricum*. J Exp Bot. **69:** 1955-1966.

Zhang, L., et al. (2017). The Tartary buckwheat genome provides insights into rutin biosynthesis and abiotic stress tolerance. Mol. Plant. **10:** 1224-1237.

Zhao, B.R., Zheng, Y., Gao, J., and Wang, X.W. (2020). Maturation of an antimicrobial peptide inhibits *Aeromonas hydrophila* infection in crayfish. J Immunol. **204:** 487-497.

Zhao, H., et al. (2022). Rewiring of the seed metabolome during Tartary buckwheat domestication. Plant Biotechnol. J. doi: 10.1111/pbi.13932.

Zhao, J., Li, L., Liu, Q., Liu, P., Li, S., Yang, D., Chen, Y., Pagnotta, S., Favery, B., Abad, P., and Jian, H. (2019). A MIF-like effector suppresses plant immunity and facilitates nematode parasitism by interacting with plant annexins. J. Exp. Bot. **70:** 5943-5958.

Zheng, A., et al. (2013). The evolution and pathogenic mechanisms of the rice sheath blight pathogen. Nat. Commun. **4:** 1424.

Zhou, M., and Memelink, J. (2016). Jasmonate-responsive transcription factors regulating plant secondary metabolism. Biotechnol Adv. **34:** 441-449.

Zhou, M., Sun, Z., Ding, M., Logacheva, M.D., Kreft, I., Wang, D., Yan, M., Shao, J., Tang, Y., Wu, Y., and Zhu, X. (2017). FtSAD2 and FtJAZ1 regulate activity of the FtMYB11 transcription repressor of the phenylpropanoid pathway in *Fagopyrum tataricum*. New Phytol. **216:** 814-828.

Zhu, Z., Zhang, F., Hu, H., Bakshi, A., Robinson, M.R., Powell, J.E., Montgomery, G.W., Goddard, M.E., Wray, N.R., Visscher, P.M., and Yang, J. (2016). Integration of summary data from GWAS and eQTL studies predicts complex trait gene targets. Nat. Genet. **48:** 481-487.

Zrenner, R., Verwaaijen, B., Genzel, F., Flemer, B., and Grosch, R. (2021). Transcriptional changes in potato sprouts upon interaction with *Rhizoctonia solani* indicate pathogen-induced interference in the defence pathways of potato. Int. J. Mol. Sci. **22:** 3094.

FIGURE LEGENDS

Figure 1 Expansion of cell wall degradation enzymes in *R. solani* AG4-HGI 3.

(A) Phylogenetic tree depicting the relationships among the genomes of 23 *R. solani* strains (left). The phylogenetic tree was reconstructed using the maximum likelihood approach based on single-copy orthogroups and rooted with *M. oryzae*. Numbers on each branch indicate the number of expanded (positive numbers) and contracted (negative number) gene families. The numbers of CAZyme genes in 23 *R. solani* isolates and *M. oryzae* are shown (right). Different colors represent different types of

CAZyme genes, with the intensity of colors being proportional to the number of genes. AA, auxiliary activity; CE, carbohydrate esterase; GT, glycosyl transferase; GH, glycoside hydrolase; CBM, carbohydrate-binding module; PL, polysaccharide lyase.
(B) Most significantly enriched GO terms of expanded gene families in *R. solani* AG4-HGI 3. Enriched pathways related to glycosyl hydrolysis and pectate lyase are shown in red. BP, Biological process; MF, Molecular function; CC, Cellular component.

Figure 2 Differentially expressed *R. solani* genes during infection of Tartary buckwheat.
(A) Venn diagram showing the number of commonly and uniquely upregulated genes from *R. solani* AG4-HGI 3 during the *R. solani*–Tartary buckwheat interaction for 6 h (RS 6 h), 14 h (RS 14 h) and 22 h (RS 22 h). Mycelial disks sub-cultured on PDA medium were used to infect the leaves of 21-day-old Tartary buckwheat seedlings for the indicated times before the leaves were harvested for transcriptome analysis. Three independent biological replicates (n = 10 seedlings each) for each treatment were conducted. Genes with P-adjusted ≤ 0.05 and fold-change > 2 (compared to non-inoculated control samples) were considered to be significantly differentially expressed genes and used for analysis. RS, *Rhizoctonia solani*.
(B) Venn diagram showing the overlap between upregulated genes encoding predicted CAZymes, effectors, secreted proteins, virulence proteins and interaction proteins in *R. solani* AG4-HGI 3 during infection of Tartary buckwheat.
(C) Most significantly enriched KEGG metabolic pathways of upregulated genes from *R. solani* AG4-HGI 3 during the infection of Tartary buckwheat by *R. solani*. Numbers next to the bars indicate the P-values.
(D) Heatmap showing the gene expression pattern of *R. solani* AG4-HGI 3 upregulated CAZyme genes involved in cellulose degradation during *R. solani* infection of Tartary buckwheat for 6 h (Rs 6 h/0 h), 14 h (Rs 14 h/0 h) and 22 h (Rs 22 h/0 h). Red and blue indicate upregulation and downregulation, respectively. Intensity of the colors is proportional to $\log_2$FC. GH, glycoside hydrolase; CBM, carbohydrate-binding module; AA, auxiliary activity; BGL, β-glucosidase; CBH, cellobiohydrolase; EGL, endoglucanase; LPMO, lytic polysaccharide monooxygenase.
(E) Phenotypes observed on N. benthamiana leaves heterologously expressing *RsYTHDC*, *RsLDCP*, *RsPRP* or *RsDAD* and infected with *R. solani* AG4-HGI 3. *N. benthamiana* leaves were inoculated with sub-cultured mycelial disks for 2 days.

Leaves transiently infiltrated with the empty vector control (EV) and then infected by *R. solani* AG4-HGI 3 were used as negative control. The phenotypes were observed in leaves of three independently infiltrated *N. benthamiana* seedlings (n = 3). The experiments were performed three times using different batches of *N. benthamiana* seedlings with similar results. Photographs of *N. benthamiana* leaves from one representative experiment are shown. Scale bars, 1 cm.

Figure 3 Differentially expressed genes from Tartary buckwheat during *R. solani* infection.

(A) Most significantly enriched KEGG metabolic pathways among differentially expressed genes of Tartary buckwheat during *R. solani* infection. The leaves of 21-day-old Tartary buckwheat seedlings were inoculated with mycelial disks sub-cultured on PDA medium for 6 h, 14 h or 22 h before being collected for transcriptome analysis. Three independent biological replicates (n = 10 seedlings each) for each treatment were conducted. Genes with P-adjusted ≤ 0.05 and fold-change >2 or < 0.5 (compared to DMSO treatment) were considered to be significantly differentially expressed genes. Numbers next to the bars indicate the P-values.

(B) Expression pattern of differentially expressed Tartary buckwheat genes related to JA biosynthesis and signaling during *R. solani* infection, shown as a heatmap of Log_2FC at the 6-h, 14-h and 22-h time points relative to the control samples. Red and blue indicate upregulation and downregulation, respectively. Intensity of the colors is proportional to the log_2FC. TGL, triacylglycerol lipase; LOX, 13-lipoxygenase; AOS, allene oxide synthase; AOC, allene oxide cyclase; OPR, (9S,13S)-12-oxo-phytodienoic acid reductase; ACOX, acyl-CoA oxidase; ACAA, 3-oxoacyl-CoA thiolase; MEP, multifunctional protein; JAR1, JASMONATE RESISTANT 1/jasmonate-amino synthetase; JAZ, JA ZIM-domain; COI1, CORONATINE INSENSITIVE 1; ERF, ETHYLENE-RESPONSIVE TRANSCRIPTION FACTOR; PR, PATHOGENESIS-RELATED.

(C) Venn diagram showing the number of Tartary buckwheat genes commonly and uniquely differentially expressed during *R. solani* infection and MeJA treatment. The leaves of 21-day-old Tartary buckwheat seedlings were inoculated with mycelial disks sub-cultured on PDA medium for 6 h (FT 6 h), 14 h (FT 14 h) or 22 h (FT 22 h), or treated with 50 μM MeJA for 1 h (JA 1 h), 4 h (JA 4 h) or 12 h (JA 12 h); the leaves were then harvested for transcriptome analysis. Three independent biological replicates

(n = 10 seedlings each) for each treatment were conducted. Genes with P-adjusted ≤ 0.05 and fold-change >2 or < 0.5 (compared to DMSO treatment for JA treatment or non-inoculated control samples for *R. solani* infection) were considered to be significantly differentially expressed genes and used for analysis. FT, *Fagopyrum tataricum*; JA, jasmonic acid.

(D) Most significantly enriched KEGG metabolic pathways of JA-induced or repressed differentially expressed genes in Tartary buckwheat during *R. solani* infection. Numbers next to the bars indicate the P-values.

Figure 4 JA-induced *FtCYP94C1* improves disease resistance of Tartary buckwheat to *R. solani* AG4-HGI 3.

(A) Phylogenetic tree illustrating the relatedness of Tartary buckwheat CYPs (Ft) to Arabidopsis CYPs (Atxg). The full-length amino acid sequences were used for phylogenetic analysis based on the neighbor-joining method. Only a subset of CYPs with high amino acid similarity to FtCYP94C1 is shown. The scale bar at the bottom represents the number of expected substitutions per site. Red represents FtCYP94C1.

(B and C) Relative *FtCYP94C1* expression levels during *R. solani* infection (B) and MeJA treatment (C). For *R. solani* infection, the leaves of 21-day-old Tartary buckwheat seedlings were inoculated with mycelial disks sub-cultured on PDA medium for 6 h, 14 h or 22 h (B), or treated with 50 μM MeJA for 1 h, 4 h or 12 h (C), and then collected for transcriptome analysis. Expression levels are estimated as FPKM values. Data show the arithmetic mean ± SD from three biological replicates (n = 10 seedlings each). Different letters indicate significant differences at adjusted $P < 0.05$ (corrected using the Benjamini-Hochberg method).

(D) Phenotype of Arabidopsis lines heterologously expressing *FtCYP94C1* and infected with *R. solani* AG4-HGI 3. The detached leaves of two-week-old Arabidopsis seedlings were inoculated with sub-cultured mycelial disks for 2 days. The Arabidopsis leaves of wild-type (Col-0) or from lines transformed with the empty vector control (EV) were used as negative controls. The phenotypes were observed in leaves of three Arabidopsis seedlings (n = 3). The experiments were performed three times using different batches of Arabidopsis seedlings. Photographs from one representative experiment are shown. Scale bars, 1 cm.

(E and F) Disease incidence (E) and disease index (F) of Arabidopsis lines heterologously expressing *FtCYP94C1* (OE1 and OE2) infected with *R. solani* AG4-

HGI 3. Leaves were treated as above, and the disease index was evaluated 2 days later. Data show the arithmetic mean ± SD from three biological replicates (n = 5). Different letters indicate significant differences at $P < 0.01$ (one-way ANOVA, Tukey's post-test). The experiment was performed three times using different batches of Arabidopsis seedlings with similar results.

(G) Arabidopsis lines heterologously expressing *FtCYP94C1* accumulate JA derivates and flavonoids. Two-week-old Arabidopsis seedlings were used for metabolite analysis. Four independent biological replicates (n = 10) for each treatment were conducted. Red and blue indicate upregulation and downregulation, respectively. Intensity of the colors is proportional to the metabolite content.

Figure 5 The integration of GWAS and transcriptomics identifies 106 genes associated with Tartary buckwheat disease resistance to *R. solani* AG4-HGI 3.

(A) Manhattan plot of the GWAS results using disease index in 320 Tartary buckwheat accessions as phenotype. Seven-day-old Tartary buckwheat seedlings were inoculated with a 50 × diluted sub-cultured mycelial solution, and the disease index was evaluated 5 days later. The mean values of disease index from three biological replicates (n = 10) for each accession were used for GWAS analysis. The red dotted line represents the significance threshold.

(B) Heatmap representation of the expression pattern of GWAS-identified genes that were both differentially expressed during infection with *R. solani* (Ft; top) and following MeJA treatment (JA; bottom). The mean FPKM values of three biological replicates (n = 10) during *R. solani* infection or MeJA treatment were used to calculate the relative expression level of these genes (shown as Log_2FC relative to non-infected for *R. solani* infection and untreated seedlings for MeJA treatment). Red and blue indicate upregulation and downregulation, respectively. Intensity of the colors is proportional to log_2FC. Genes used in transgenic experiments are outlined with dotted lines. *FtPG1*, polygalacturonase-like, FtPinG0100647900; *FtADH1*, alcohol dehydrogenase-like 1, *FtPinG0302737400*; *FtASP,* aspartic proteinase, FtPinG0302743900*;* *FtCSLG2*, cellulose synthase-like protein G2, FtPinG0404615400; *FtKCS11*, 3-ketoacyl-CoA synthase 11-like, FtPinG0708058700; *FtCES18*, probable carboxylesterase 18, FtPinG0809058900.

Figure 6 JA-induced *FtASP* improves disease resistance of Tartary buckwheat to *R. solani* AG4-HGI 3.

(A) Box plots of the disease index in Tartary buckwheat accessions harboring the C-haplotype (53 accessions), the T-haplotype (210 accessions) and the Y(C/T)-haplotype (54 accessions). The data are based on the mean disease index values from three biological replicates (n = 10) for each accession. *P < 0.05 and ****P < 0.0001, as calculated using two-tailed Student's t-test.

(B) Relative *FtASP* expression levels in different Tartary buckwheat accessions. The mean values from three biological replicates (n = 10) for each accession were used for analysis. The formula, r value and P-value of the regression line were shown.

(C) Phylogenetic tree for ASP proteins using full-length amino acid sequences from Tartary buckwheat (FtASP) and other plants. The phylogenetic tree was reconstructed using the neighbor-joining method. Only a subset of ASPs with high amino acid similarity to FtASP is shown. The scale bar at the bottom represents the number of expected substitutions per site. Red represents FtASP.

(D and E) Incidence (D) and disease index (E) of Arabidopsis lines heterologously expressing *FtASP* (OE1, OE2 and OE3) infected with *R. solani* AG4-HGI 3. The detached leaves of two-week-old Arabidopsis seedlings were inoculated with the sub-cultured mycelial disks, and the disease index was evaluated after 2 days. The Arabidopsis leaves of wild-type (Col-0) and lines transformed with the empty vector control (EV) were used as negative controls. Data show the arithmetic mean ± SD from three biological replicates (n = 5 seedlings each). Different letters indicate significant differences at P < 0.01 (one-way ANOVA, Tukey's post-test). The experiment was performed three times using different batches of Arabidopsis seedlings with similar results.

(F) Phenotype of Arabidopsis lines heterologously expressing *FtASP* infected with *R. solani* AG4-HGI 3. Leaves were treated as above. Phenotypes were observed from the leaves of three Arabidopsis seedlings (n = 3). The experiment was performed three times using different batches of Arabidopsis seedlings. Photographs from one representative experiment are shown. Scale bars, 1 cm.

(G) Inhibitory effect of recombinant FtASP (1-225), FtASP-N (1-112) and FtASP-C (113-225) proteins on the growth of *R. solani* AG4-HGI 3. Purified recombinant proteins were added to PDB medium pre-inoculated with *R. solani* AG4-HGI 3. The effects of each recombinant protein was evaluated after culture for 2 days. The

phenotypes were observed in three biological replicates (n = 3). The experiment was performed three times using different batches of purified recombinant proteins with similar results. Photographs from one representative experiment are shown.

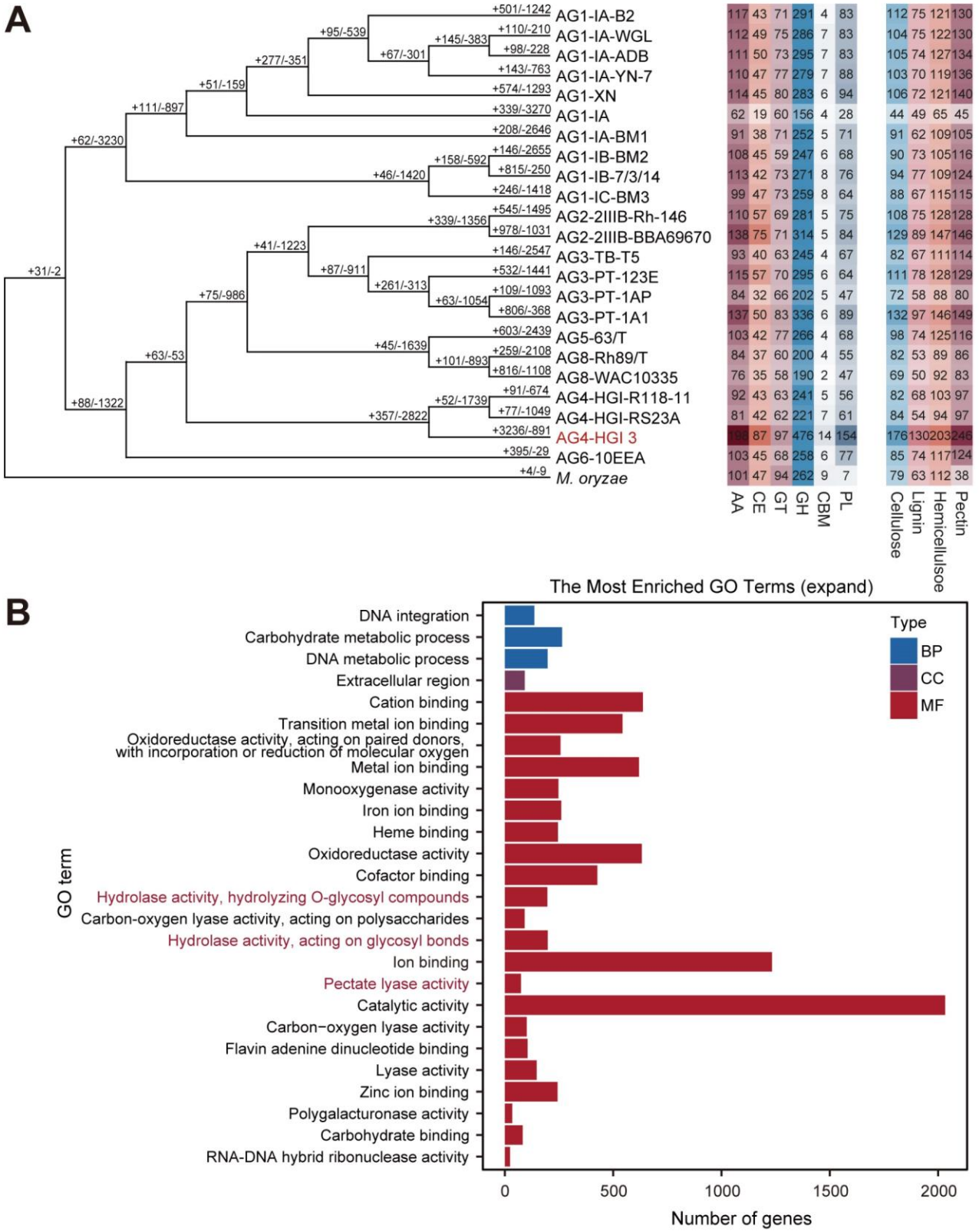

Figure 1 Expansion of cell wall degradation enzymes in *R. solani* AG4-HGI 3.

(A) Phylogenetic tree depicting the relationships among the genomes of 23 *R. solani* strains (left). The phylogenetic tree was reconstructed using the maximum likelihood approach based on single-copy orthogroups and rooted with *M. oryzae*. Numbers on each branch indicate the number of expanded (positive numbers) and contracted (negative number) gene families. The numbers of CAZyme genes in 23 *R. solani* isolates and *M. oryzae* are shown (right). Different colors represent different types of CAZyme genes, with the intensity of colors being proportional to the number of genes. AA, auxiliary activity; CE, carbohydrate esterase; GT, glycosyl transferase; GH, glycoside hydrolase; CBM, carbohydrate-binding module; PL, polysaccharide lyase.

(B) Most significantly enriched GO terms of expanded gene families in *R. solani* AG4-HGI 3. Enriched pathways related to glycosyl hydrolysis and pectate lyase are shown in red. BP, Biological process; MF, Molecular function; CC, Cellular component.

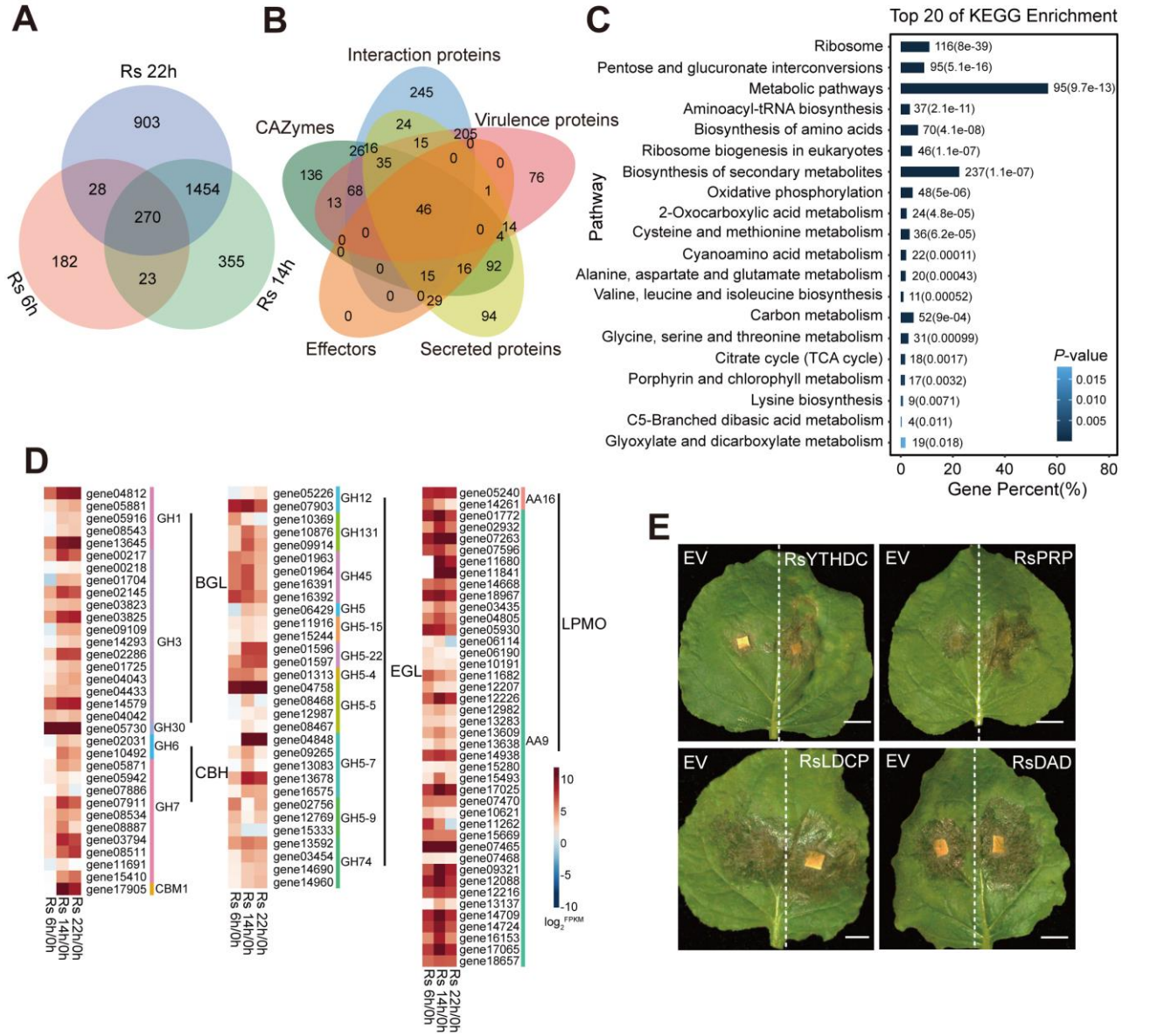

Figure 2 Differentially expressed *R. solani* genes during infection of Tartary buckwheat.

(A) Venn diagram showing the number of commonly and uniquely upregulated genes from *R. solani* AG4-HGI 3 during the *R. solani*–Tartary buckwheat interaction for 6 h (RS 6 h), 14 h (RS 14 h) and 22 h (RS 22 h). Mycelial disks sub-cultured on PDA medium were used to infect the leaves of 21-day-old Tartary buckwheat seedlings for the indicated times before the leaves were harvested for transcriptome analysis. Three independent biological replicates (n = 10 seedlings each) for each treatment were conducted. Genes with P-adjusted ≤ 0.05 and fold-change > 2 (compared to non-inoculated control samples) were considered to be significantly differentially expressed genes and used for analysis. RS , *Rhizoctonia solani*.

(B) Venn diagram showing the overlap between upregulated genes encoding predicted CAZymes, effectors, secreted proteins, virulence proteins and interaction proteins in *R. solani* AG4-HGI 3 during infection of Tartary buckwheat.

(C) Most significantly enriched KEGG metabolic pathways of upregulated genes from *R. solani* AG4-HGI 3 during the infection of Tartary buckwheat by *R. solani*. Numbers next to the bars indicate the *P*-values.

(D) Heatmap showing the gene expression pattern of *R. solani* AG4-HGI 3 upregulated CAZyme genes involved in cellulose degradation during *R. solani* infection of Tartary buckwheat for 6 h (Rs 6 h/0 h), 14 h (Rs 14 h/0 h) and 22 h (Rs 22 h/0 h). Red and blue indicate upregulation and downregulation, respectively. Intensity of the colors is proportional to $\log_2$FC. GH, glycoside hydrolase; CBM, carbohydrate-binding module; AA, auxiliary activity; BGL, β-glucosidase; CBH, cellobiohydrolase; EGL, endoglucanase; LPMO, lytic polysaccharide monooxygenase.

(E) Phenotypes observed on N. benthamiana leaves heterologously expressing *RsYTHDC*, *RsLDCP*, *RsPRP* or *RsDAD* and infected with *R. solani* AG4-HGI 3. *N. benthamiana* leaves were inoculated with sub-cultured mycelial disks for 2 days. Leaves transiently infiltrated with the empty vector control (EV) and then infected by *R. solani* AG4-HGI 3 were used as negative control. The phenotypes were observed in leaves of three independently infiltrated *N. benthamiana* seedlings (n = 3). The experiments were performed three times using different batches of *N. benthamiana* seedlings with similar results. Photographs of *N. benthamiana* leaves from one representative experiment are shown. Scale bars, 1 cm.

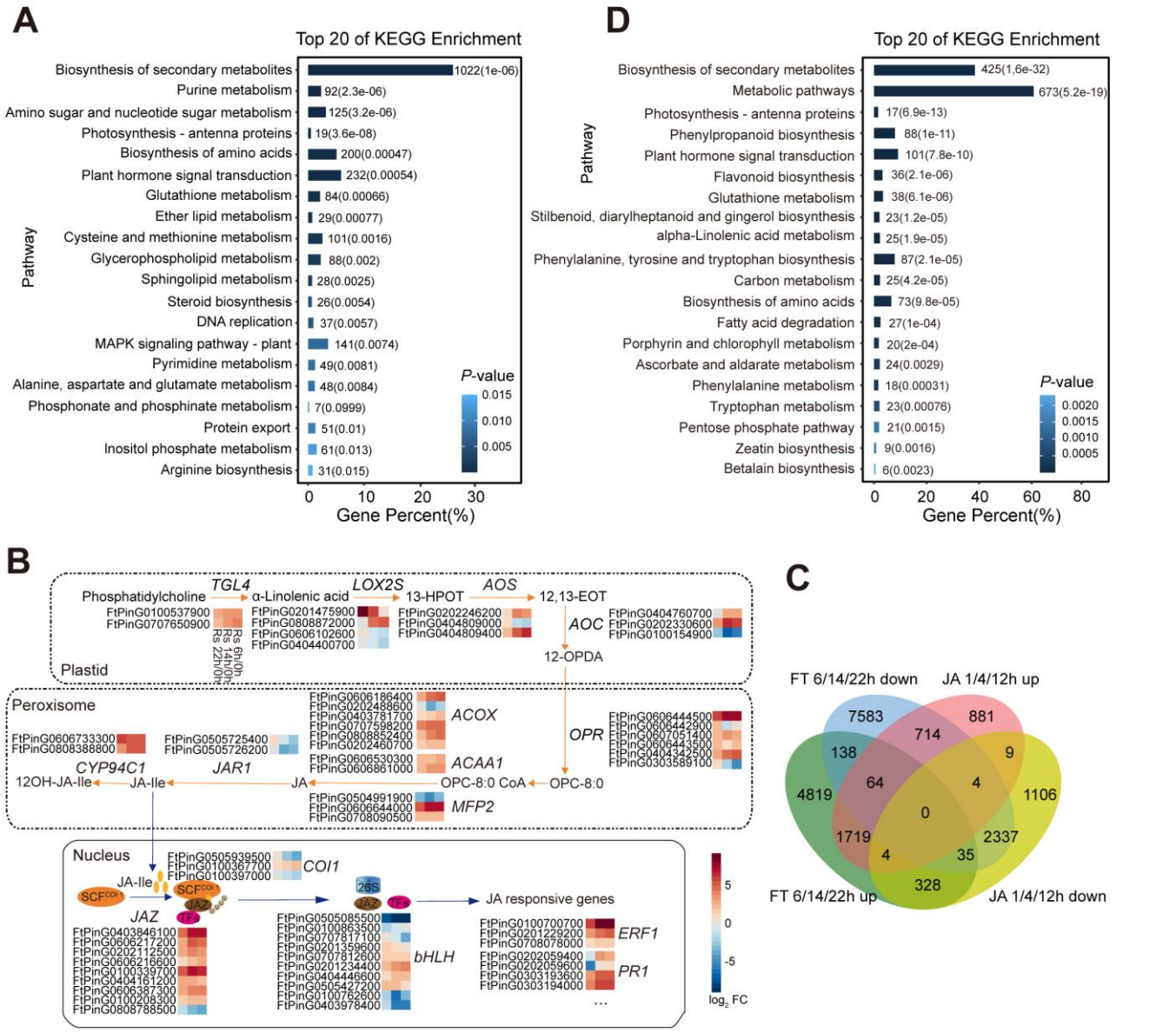

Figure 3 Differentially expressed genes from Tartary buckwheat during *R. solani* infection.

(A) Most significantly enriched KEGG metabolic pathways among differentially expressed genes of Tartary buckwheat during *R. solani* infection. The leaves of 21-day-old Tartary buckwheat seedlings were inoculated with mycelial disks sub-cultured on PDA medium for 6 h, 14 h or 22 h before being collected for transcriptome analysis. Three independent biological replicates (n = 10 seedlings each) for each treatment were conducted. Genes with P-adjusted ≤ 0.05 and fold-change >2 or < 0.5 (compared to DMSO treatment) were considered to be significantly differentially expressed genes. Numbers next to the bars indicate the P-values.

(B) Expression pattern of differentially expressed Tartary buckwheat genes related to JA biosynthesis and signaling during *R. solani* infection, shown as a heatmap of Log_2FC at the 6-h, 14-h and 22-h time points relative to the control samples. Red and blue indicate upregulation and downregulation, respectively. Intensity of the colors is proportional to the log_2FC. TGL, triacylglycerol lipase; LOX, 13-lipoxygenase; AOS, allene oxide synthase; AOC, allene oxide cyclase; OPR, (9S,13S)-12-oxo-phytodienoic acid reductase; ACOX, acyl-CoA oxidase; ACAA, 3-oxoacyl-CoA thiolase; MEP, multifunctional protein; JAR1, JASMONATE RESISTANT 1/jasmonate-amino synthetase; JAZ, JA ZIM-domain; COI1, CORONATINE INSENSITIVE 1; ERF, ETHYLENE-RESPONSIVE TRANSCRIPTION FACTOR; PR, PATHOGENESIS-RELATED.

(C) Venn diagram showing the number of Tartary buckwheat genes commonly and uniquely differentially expressed during *R. solani* infection and MeJA treatment. The leaves of 21-day-old Tartary buckwheat seedlings were inoculated with mycelial disks sub-cultured on PDA medium for 6 h (FT 6 h), 14 h (FT 14 h) or 22 h (FT 22 h), or treated with 50 μM MeJA for 1 h (JA 1 h), 4 h (JA 4 h) or 12 h (JA 12 h); the leaves were then harvested for transcriptome analysis. Three independent biological replicates (n = 10 seedlings each) for each treatment were conducted. Genes with P-adjusted ≤ 0.05 and fold-change >2 or < 0.5 (compared to DMSO treatment for JA treatment or non-inoculated control samples for *R. solani* infection) were considered to be significantly differentially expressed genes and used for analysis. FT, *Fagopyrum tataricum*; JA, jasmonic acid.

(D) Most significantly enriched KEGG metabolic pathways of JA-induced or repressed differentially expressed genes in Tartary buckwheat during *R. solani* infection. Numbers next to the bars indicate the P-values.

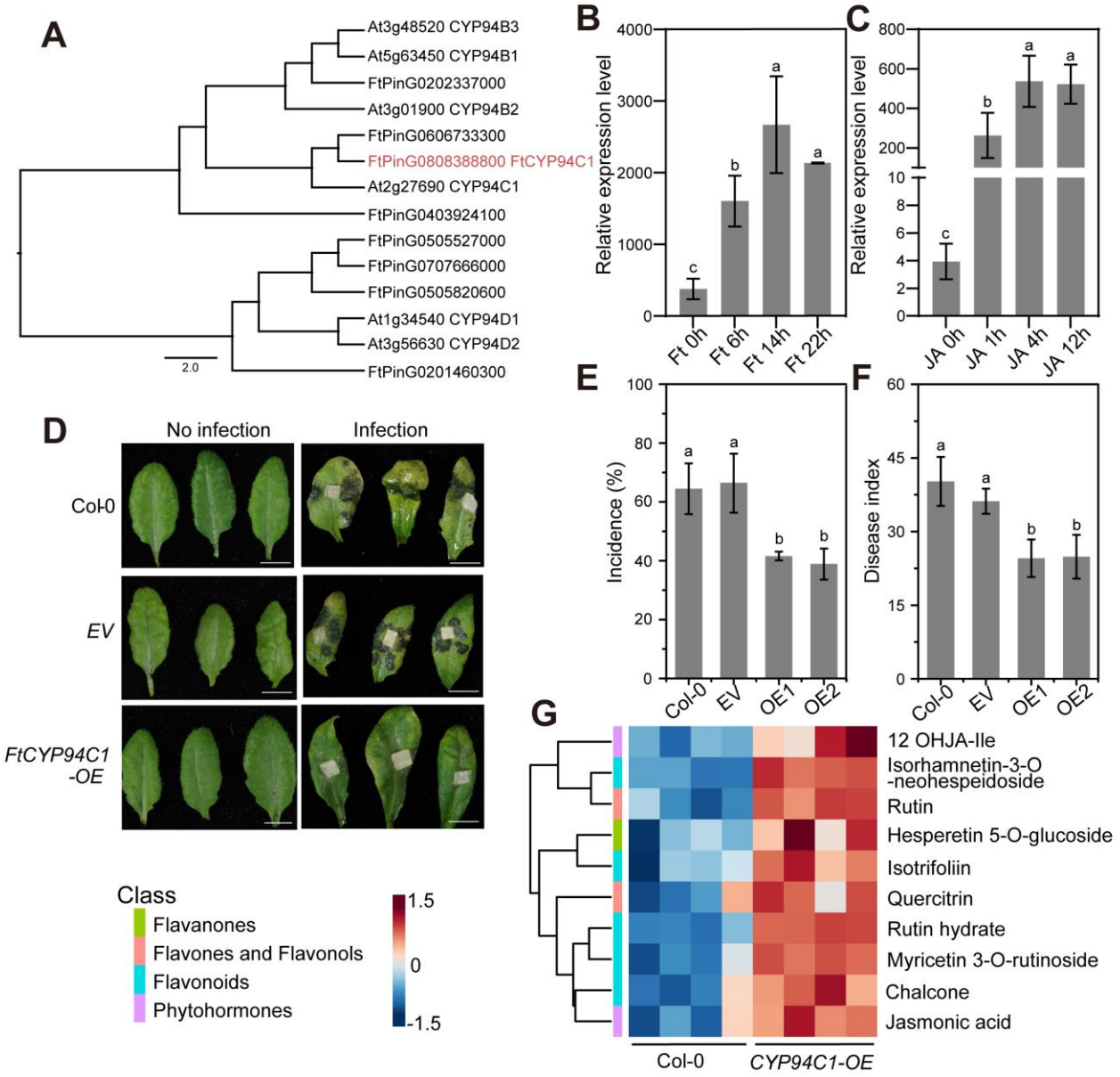

Figure 4 JA-induced *FtCYP94C1* improves disease resistance of Tartary buckwheat to *R. solani* AG4-HGI 3.
(A) Phylogenetic tree illustrating the relatedness of Tartary buckwheat CYPs (Ft) to Arabidopsis CYPs (At xg). The full-length amino acid sequences were used for phylogenetic analysis based on the neighbor-joining method. Only a subset of CYPs with high amino acid similarity to FtCYP94C1 is shown. The scale bar at the bottom represents the number of expected substitutions per site. Red represents FtCYP94C1 .
(B and C) Relative *FtCYP94C1* expression levels during *R. solani* infection (B) and MeJA treatment (C). For *R. solani* infection, the leaves of 21-day-old Tartary buckwheat seedlings were inoculated with mycelial disks sub-cultured on PDA medium for 6 h, 14 h or 22 h (B), or treated with 50 μM MeJA for 1 h, 4 h or 12 h (C), and then collected for transcriptome analysis. Expression levels are estimated as FPKM values. Data show the arithmetic mean ± SD from three biological replicates (n = 10 seedlings each). Different letters indicate significant differences at adjusted $P < 0.05$ (corrected using the Benjamini-Hochberg method).
(D) Phenotype of Arabidopsis lines heterologously expressing *FtCYP94C1* and infected with *R. solani* AG4-HGI 3. The detached leaves of two-week-old Arabidopsis seedlings were inoculated with sub-cultured mycelial disks for 2 days. The Arabidopsis leaves of wild-type (Col-0) or from lines transformed with the empty vector control (EV) were used as negative controls. The phenotypes were observed in leaves of three Arabidopsis seedlings (n = 3). The experiments were performed three times using different batches of Arabidopsis seedlings. Photographs from one representative experiment are shown. Scale bars, 1 cm.
(E and F) Disease incidence (E) and disease index (F) of Arabidopsis lines heterologously expressing *FtCYP94C1* (OE1 and OE2) infected with *R. solani* AG4-HGI 3. Leaves were treated as above, and the disease index was evaluated 2 days later. Data show the arithmetic mean ± SD from three biological replicates (n = 5). Different letters indicate significant differences at $P < 0.01$ (one-way ANOVA, Tukey's post-test). The experiment was performed three times using different batches of Arabidopsis seedlings with similar results.
(G) Arabidopsis lines heterologously expressing *FtCYP94C1* accumulate JA derivates and flavonoids. Two-week-old Arabidopsis seedlings were used for metabolite analysis. Four independent biological replicates (n = 10) for each treatment were conducted. Red and blue indicate upregulation and downregulation, respectively. Intensity of the colors is proportional to the metabolite content.

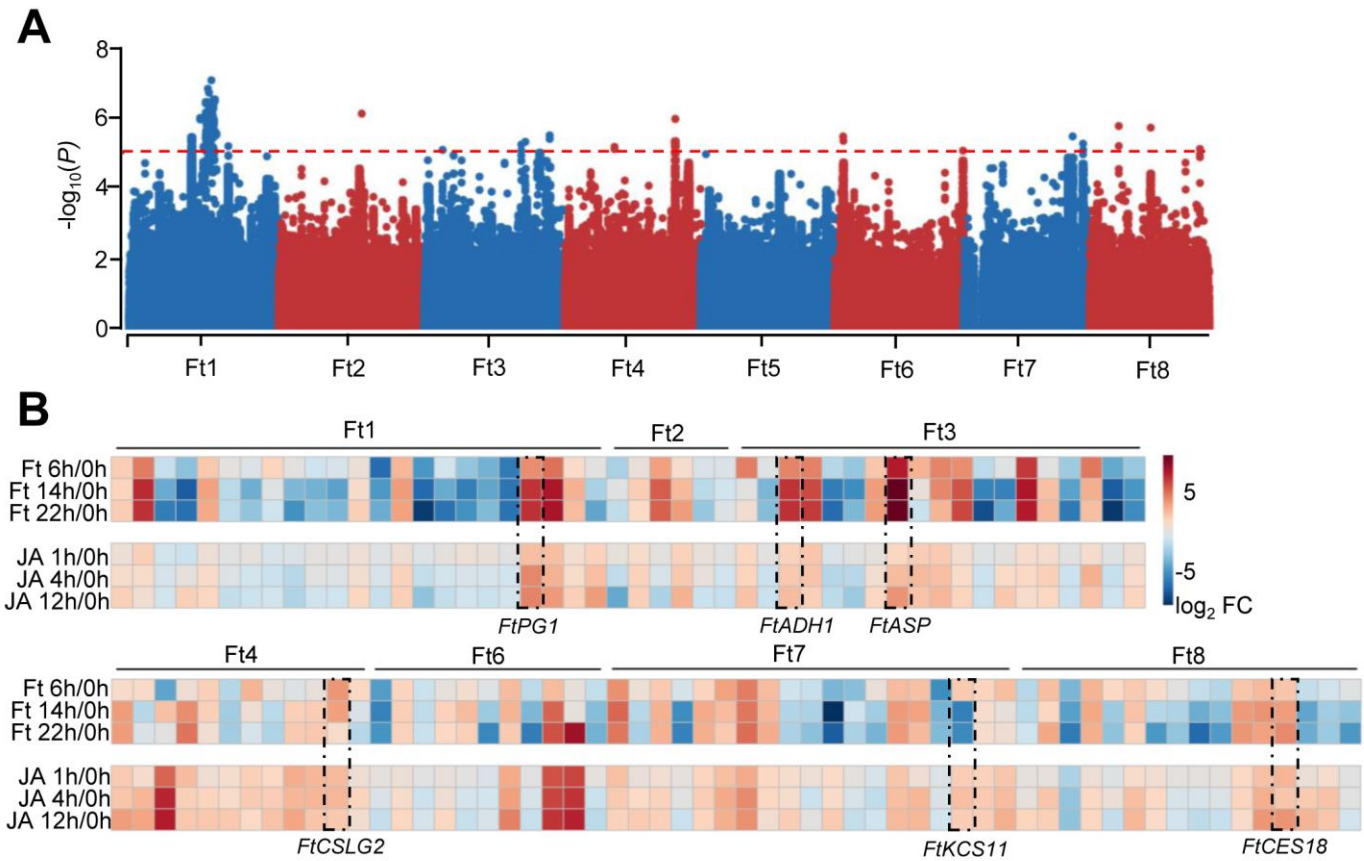

Figure 5 The integration of GWAS and transcriptomics identifies 106 genes associated with Tartary buckwheat disease resistance to *R. solani* AG4-HGI 3.

(A) Manhattan plot of the GWAS results using disease index in 320 Tartary buckwheat accessions as phenotype. Seven-day-old Tartary buckwheat seedlings were inoculated with a 50 × diluted sub-cultured mycelial solution, and the disease index was evaluated 5 days later. The mean values of disease index from three biological replicates (*n* = 10) for each accession were used for GWAS analysis. The red dotted line represents the significance threshold.

(B) Heatmap representation of the expression pattern of GWAS-identified genes that were both differentially expressed during infection with *R. solani* (Ft; top) and following MeJA treatment (JA; bottom). The mean FPKM values of three biological replicates (*n* = 10) during *R. solani* infection or MeJA treatment were used to calculate the relative expression level of these genes (shown as Log_2FC relative to non-infected for *R. solani* infection and untreated seedlings for MeJA treatment). Red and blue indicate upregulation and downregulation, respectively. Intensity of the colors is proportional to log_2FC. Genes used in transgenic experiments are outlined with dotted lines. *FtPG1*, polygalacturonase-like, FtPinG0100647900; *FtADH1*, alcohol dehydrogenase-like 1, *FtPinG0302737400*; *FtASP,* aspartic proteinase*,* FtPinG0302743900*; FtCSLG2*, cellulose synthase-like protein G2, FtPinG0404615400; *FtKCS11*, 3-ketoacyl-CoA synthase 11-like, FtPinG0708058700; *FtCES18*, probable carboxylesterase 18, FtPinG0809058900.

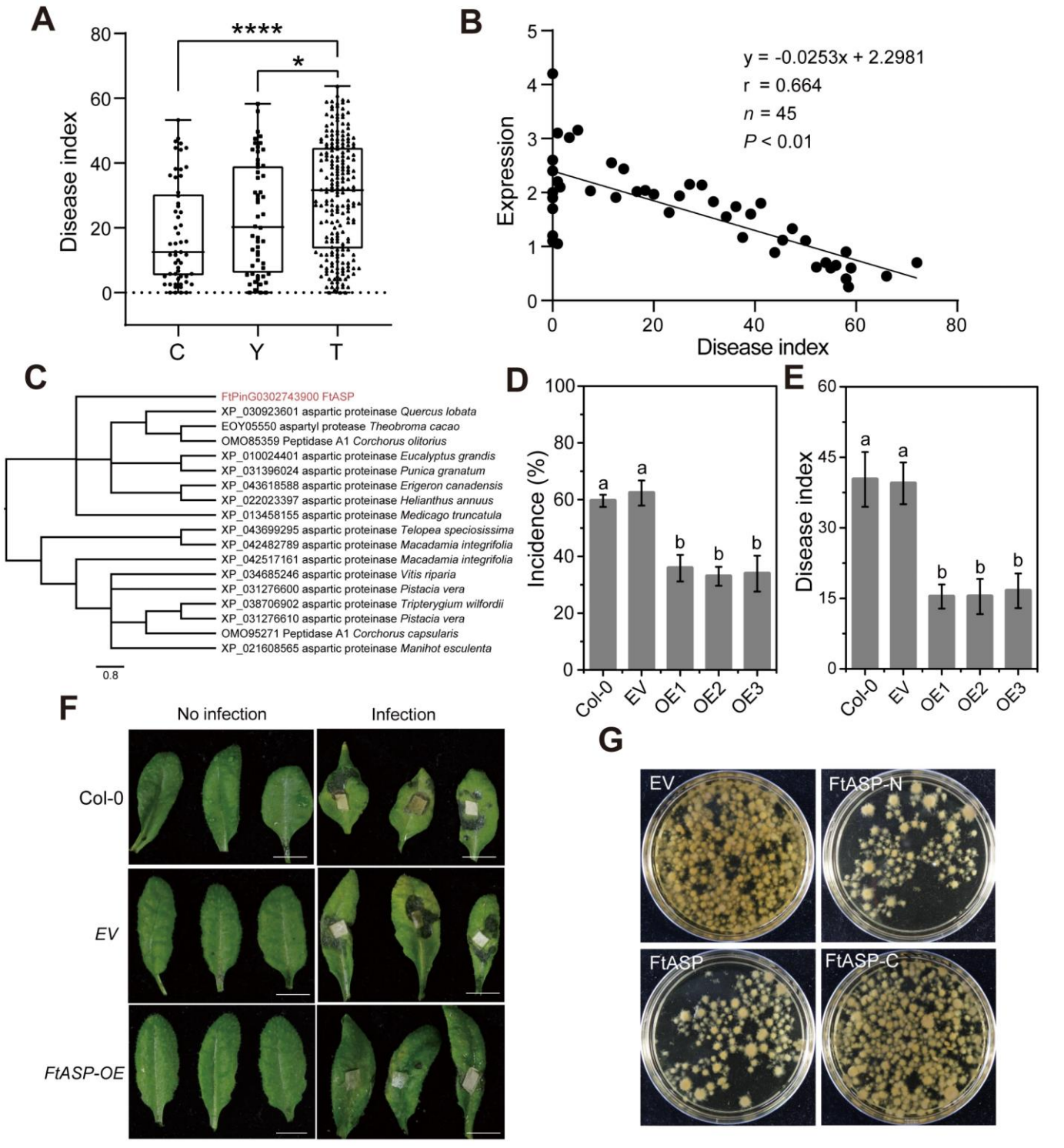

Figure 6 JA-induced *FtASP* improves disease resistance of Tartary buckwheat to *R. solani* AG4-HGI 3.

(A) Box plots of the disease index in Tartary buckwheat accessions harboring the C-haplotype (53 accessions), the T-haplotype (210 accessions) and the Y(C/T)-haplotype (54 accessions). The data are based on the mean disease index values from three biological replicates (n = 10) for each accession. *P < 0.05 and ****P < 0.0001, as calculated using two-tailed Student's t-test.
(B) Relative *FtASP* expression levels in different Tartary buckwheat accessions. The mean values from three biological replicates (n = 10) for each accession were used for analysis. The formula, r value and P-value of the regression line were shown.
(C) Phylogenetic tree for ASP proteins using full-length amino acid sequences from Tartary buckwheat (FtASP) and other plants. The phylogenetic tree was reconstructed using the neighbor-joining method. Only a subset of ASPs with high amino acid similarity to FtASP is shown. The scale bar at the bottom represents the number of expected substitutions per site. Red represents FtASP.
(D and E) Incidence (D) and disease index (E) of Arabidopsis lines heterologously expressing *FtASP* (OE1, OE2 and OE3) infected with *R. solani* AG4-HGI 3. The detached leaves of two-week-old Arabidopsis seedlings were inoculated with the sub-cultured mycelial disks, and the disease index was evaluated after 2 days. The Arabidopsis leaves of wild-type (Col-0) and lines transformed with the empty vector control (EV) were used as negative controls. Data show the arithmetic mean ± SD from three biological replicates (n = 5 seedlings each). Different letters indicate significant differences at P < 0.01 (one-way ANOVA, Tukey's post-test). The experiment was performed three times using different batches of Arabidopsis seedlings with similar results.
(F) Phenotype of Arabidopsis lines heterologously expressing *FtASP* infected with *R. solani* AG4-HGI 3. Leaves were treated as above. Phenotypes were observed from the leaves of three Arabidopsis seedlings (n = 3). The experiment was performed three times using different batches of Arabidopsis seedlings. Photographs from one representative experiment are shown. Scale bars, 1 cm.
(G) Inhibitory effect of recombinant FtASP (1-225), FtASP-N (1-112) and FtASP-C (113-225) proteins on the growth of *R. solani* AG4-HGI 3. Purified recombinant proteins were added to PDB medium pre-inoculated with *R. solani* AG4-HGI 3. The effects of each recombinant protein was evaluated after culture for 2 days. The phenotypes were observed in three biological replicates (n = 3). The experiment was performed three times using different batches of purified recombinant proteins with similar results. Photographs from one representative experiment are shown.